UTRECHT UNIVERSITY

Cross-shore sand transport in shallow water

Wetering, J.A.M. van de (3713261)

MSc Thesis

Under the supervision of

Prof. Dr. B.G. Ruessink

MSc. J.A. Brinkkemper

Department of Physical Geography

Faculty of Geosciences

Utrecht University

The Netherlands

Abstract

The temporal and spatial variations in the relative importance of three primary suspended transport components (high frequency and low frequency oscillatory, and steady current driven transport) were examined, in an attempt to explain onshore sandbar migration. The data came from a three week field campaign carried out in the inner surf zone of Vejers beach, Denmark, during which periods of low energetic swell and mild energetic wave conditions (resulting in onshore migration), and a storm event (causing offshore sandbar migration) were experienced. Almost exclusively net offshore directed transport, dominated by undertow driven transport, was recorded during high tide throughout the field campaign. For (non-breaking) swell conditions it was found that the importance of this steady transport component on net transport reduces in comparison to both oscillatory transport components, with increasing water depth and increased distance from the shoreline. Adversely, for mild and high energetic wave conditions the steady component rather increased in importance with increasing water depth and increased distance from the shoreline. A non-dimensional parameter was analysed on its ability to predict net onshore directed transport. It was found that it was a reliable indicator for the relative importance of the oscillatory components compared to the steady component, but not their direction. Only in shallow water (< 0.8 m), close to the shoreline (< 30 m), was there a tendency for both oscillatory currents to be onshore directed, which occasionally allowed for net onshore directed transport. Since the data gathered during mid to high tide was almost solely offshore directed, it is thought that enough onshore directed transport must have taken place during the shallow water and sheet flow conditions of low tide to compensate for this predominance of net offshore directed transport and allow for the onshore migration of sandbars.

Contents

1 Introduction

1.1 Motivation

Sandbars in the surf zone are known to be vitally important for the protection of the beach against wave attack through increased wave energy dissipation. Onshore migration of these bars, which is said to occur under mild energetic wave conditions, may result in the bars becoming attached to the beach, thus increasing the sand budget of the beach. This is especially important for the preservation of the beach as it may experience degradation during high energetic wave conditions of storm events. The causes of this shoreward sandbar migration, which is found to predominantly take place under low to moderate energetic wave conditions, are not yet well understood. For example, in various literature it is recognized that current models, which attempt to simulate the cross-shore sediment transport and corresponding beach morphology, fail to accurately predict bar migration under various wave conditions, either by undervaluing the amount of onshore sediment transport or even incorrectly predicting offshore bar migrating during moderate wave conditions (e.g. Thornton and Humiston, 1996).

To contribute to our understanding of sandbar migration and improve existing models of shore face development it seems vitally important to analyse not only the (relative importance of) sediment transport mechanisms, but also their time variability with respect to various beach and wave/water characteristics. Since sediment used for berm formation and beach recovery (after large storm events) comes predominantly from the surf zone (Jensen et al., 2009), and it is said that the direction of net sediment transport rates in this surf zone determines whether beach accretion or offshore bar migration takes place, the mechanisms of the sediment transport processes in the surf zone are clearly of interest.

1.2 Pre-existing knowledge

Since as early as 1992 (Osborne and Greenwood, a/b) literature has explored the idea of splitting the net cross-shore suspended sand transport up in separate transport components, based on the difference in the mechanisms that drive the transport. Generally, oscillatory currents driven transport and mean currents driven steady transport components are found to be the predominant contributors. The transport due to oscillatory currents is occasionally further divided through spectral analysis into a high frequency component associated with wind-forced waves and a low frequency component generated by infragravity waves.

The balance between these components determines the direction of the net transport, which has been reported to depend in part on the energy level of the waves.

During high energetic wave conditions such as storm events, which are most frequently experienced during the winter season, intense wave breaking takes place on bar crests as a result of large relative wave heights. This subsequently drives strong offshore-directed currents in the form of undertow which carry sediment from the beach front and shoreface in seaward direction, resulting in offshore migration of the sandbars (Hoefel and Elgar, 2003) and subsequently far offshore positioned sandbars and a straight, low sloping “storm” or “winter” profile (see Figure 1.1). Adversely, under low and moderate energetic wave conditions, as is common during the summer season and the fair weather in-between storm events, onshore sediment transport takes place. This as a result of the undertow-induced

offshore sediment transport being balanced out by a slower wave-induced onshore transport. These conditions are often associated with relatively long period (swell) waves which end up plunging in the shallow waters of the upper shoreface or near bar crests (Aagaard and Hughes, 2010). Onshore sandbar migration takes place under these conditions, which allows the beach to recover (a portion) of the sediment lost during the previous storm event.

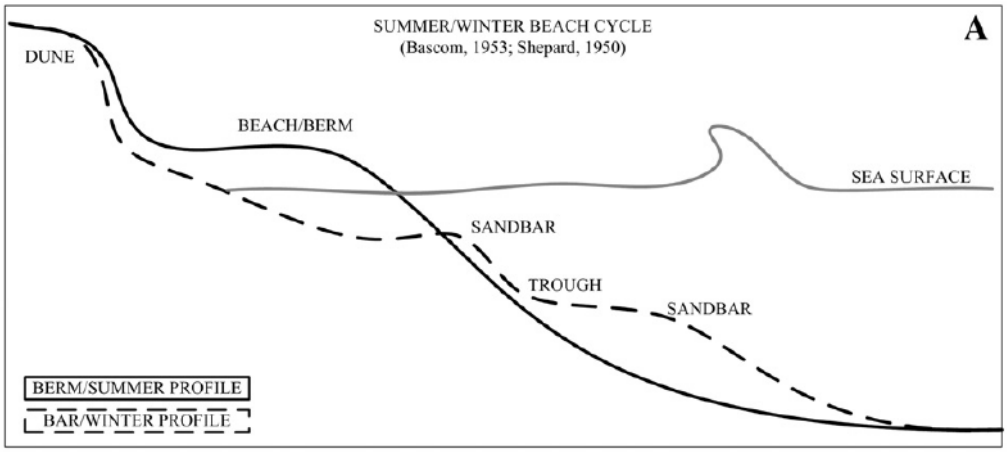

Figure 1.1: Classic beach cycle model composed of bar-type (winter) and berm-type (summer) profiles (modified from Komar, 1998). (Source: Roberts et al., 2013)

1.3 Introduction to field campaign

Some initial progress has been made in analysing the spatial and temporal variability of the various cross-shore transport mechanisms during storm conditions and on dissipative beaches. In previous research the surf zone transport fluxes have been attributed to hydrodynamics and offshore sandbar migration has been qualitatively linked to cross-shore transport gradients in the vicinity of the sandbar. To compliment previous findings a new research project dubbed the TASTI field experiment (abbreviation to Turbulence And Sand Transport Initiative) was carried out, conjoining multiple individual (master) research projects from both Utrecht University and University of Copenhagen. Through a 23 day field campaign, in which multiple rigs were deployed equipped with various sensors to measure flow velocity, suspended sand concentration, and pressure, a new and unique dataset was established. This research project intended to analyse processes in the shallow, inner surf zone which is where the exchange of sand with the beach takes place (Masselink and Puleo, 2006). Moreover, the project set out to gather data during low to moderate energetic wave conditions which are expected to result in onshore sand transport and sandbar migration, as well as cause longshore variability in the sandbars and shoreline.

The large amount of data, gathered over an extended period of time enables a focus of the data analysis on the temporal variability of the various processes in the inner surf zone. Additionally, the deployment of three frames set up alternatingly with 5 pressure sensors along a cross-shore transect, combined with daily documentation of the nearshore profile, allows for a detailed analysis on spatial gradients in hydrodynamics, morphology and sand transport.

1.4 Reading guide

With this thesis project an attempt is made to add additional information on the distribution of transport processes, particularly in the shallow surf zone and during both low to moderate energetic swell and sea wave and high energetic storm conditions, in order to supplement previous findings.
In the report at hand all aspects of the research are described. In section 2 a literature study is presented which provides background information on various processes that take place in the nearshore region and the three listed transport mechanisms. Additionally, findings of previous studies on the subject of cross-shore transport and sandbar migration will be cited, and the research questions for this project are given. Section 3 consists of the methodology. The results are shown in section 4 and subsequently discussed in section 5; i.a. comparing the results with the findings of previous research. Additionally, recommendations for future research are given. A summary of the conclusions can be found in section 6.

2 Literature study

2.1 Background information on the transport components

2.1.1 Sediment transport due to incident waves

Throughout the shoaling zone sea/swell waves assume a skewed wave shape; the wave crests become more narrow and higher while the wave troughs broader and shallower. Once the incident waves reach shallow enough waters in the surf zone, they start to break during which their shape transforms further, generally becoming increasingly more asymmetric as they travel further through the surf zone in landward direction. The resulting sawtooth-like wave shape has a characteristic gradual slope from crest to trough, but a steep slope from trough back to crest.

The shape of the waves at the water surface does affect the orbital motion underneath it. The oscillatory currents in this orbital motion subsequently influences the direction in which and the amount of sediment that is transported. For skewed waves, the velocities underneath the wave crests are much larger than under the trough, which allows for coarser material to be transported in onshore direction under the crests but which can not be moved in offshore direction under the wave trough, thus resulting in time averaged net onshore directed transport. For asymmetric shaped waves the phase lag effect between concentration and velocity becomes an important aspect of the transport. Sawtooth-like waves means that most of the sediment is stirred near the end of the trough and the beginning of the crest. Due to the limited time between trough and crest, a large portion of the sediment stirred during the trough is still suspended when velocity reversal takes place, and is subsequently transported in onshore direction. Adversely, most of the sediment stirred under the crest has enough time to be transported under the crest and settle before the next velocity reversal takes place. Therefore, time averaged transport by asymmetric waves is onshore favoured (Ruessink et al., 2011).

2.1.2 Sediment transport due to infragravity waves

Infragravity wave have been known to be a significant contributor to cross-shore suspended sand transport. Particularly at high energetic (storm) conditions, during which the infragravity wave amplitude can be quite large in the inner surf zone, may infragravity wave driven transport be comparative in magnitude and potentially even exceed the transport induced by mean currents (Russell, 1993). Infragravity wave currents are, similar to wind-wave currents, oscillatory in nature. Therefore, time averaged transport attributed to infragravity waves is a result of differences in the amount of sand stirred during the crest and trough of these long period waves. However, since infragravity waves are generally incapable of resuspending sand particles from the seabed and therefore rely on wind-waves for the stirring of sand, the direction of infragravity wave driven transport is ultimately determined by the coupling between the (bound) infragravity waves and the wave groups (see Figure 2.1). For bound infragravity waves the wave signal is out of phase with the wave group signal with long wave troughs where the waves in the wave group are highest. As these highest waves cause more stirring than the lowest waves, found during the infragravity wave crests, the bound infragravity wave induced cross-shore transport is subsequently seaward directed (Ruessink et al., 1998).

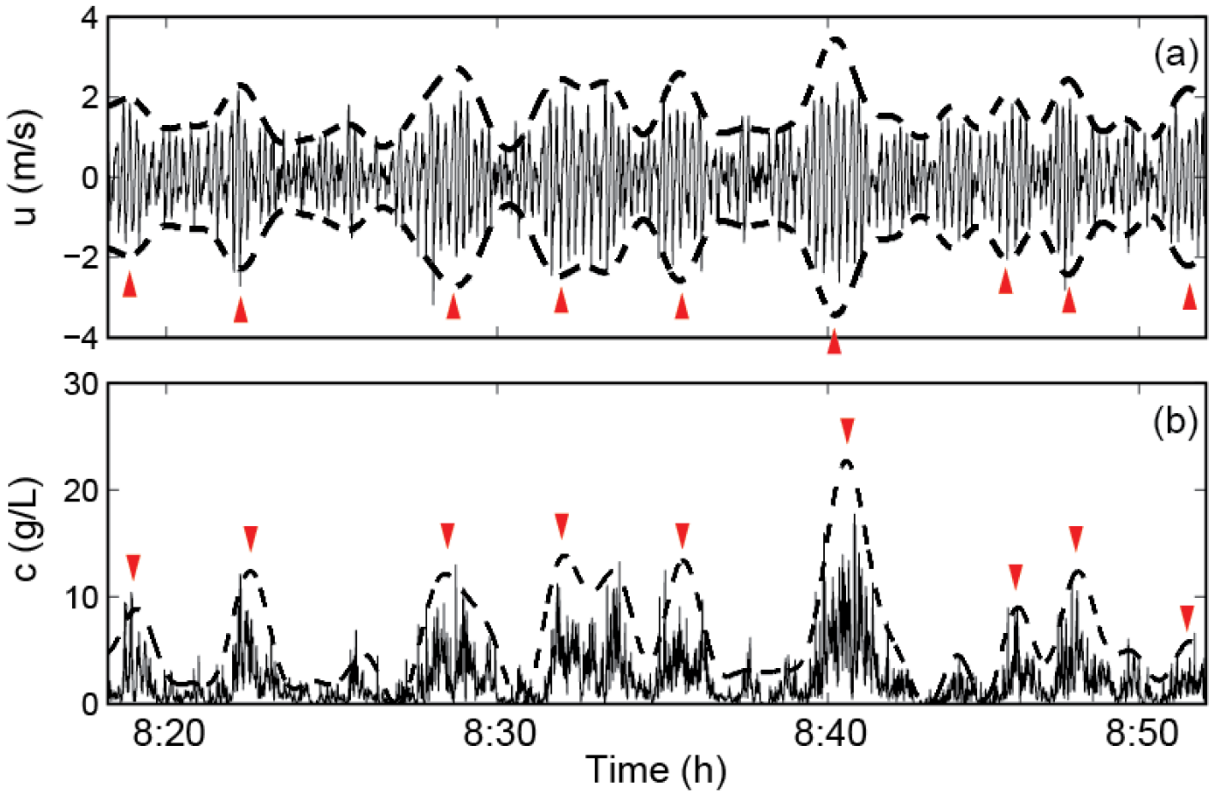

Figure 2.1: Time series of (a) cross-shore current velocity u ($z = 0.25$ m; solid line) and the envelope function of u (thick, dashed lines); and (b) suspended sediment concentration c ($z = 0.05$ m; solid line) and low-pass-filtered c (thick dashed line) (just outside of the breaker line, over a flat bed, Mullaloo Beach, Western Australia). (source: Kularatne and Pattiaratchi, 2014)

Shown from field data (Masselink, 1995), numerically (List, 1992) and theoretically (Janssen et al., 2003) this phase difference shifts away from 180 degrees as the waves reach the breaker zone, causing the (unbound) infragravity wave to lag behind its associated wave group. This phase shift continues to increase as the waves travel further towards the coast, while the wave groupiness falls apart, subsequently altering the coupling between the long wave crests and troughs and amplified suspended sand concentrations. This may not only affect the magnitude of time averaged infragravity transport, but also its direction. This, in part, causes the direction of infragravity wave driven transport to be inconsistent across the shoreface.

2.1.3 Sediment transport due to mean currents

Mean currents are generated by local pressure gradients caused by elevations or depressions in the mean water surface. They are similar to infragravity waves in that they generally depend on incident waves for sediment suspension so that it can be transported. Only when there is a strong mean current in the form of a rip current present are the resulting shear stress large enough to result in sand stirring. Such rip currents are only present when there is significant longshore variability in the nearshore morphology. Rip currents will result in large, but localized, offshore directed transport fluxes (see Figure 2.2).

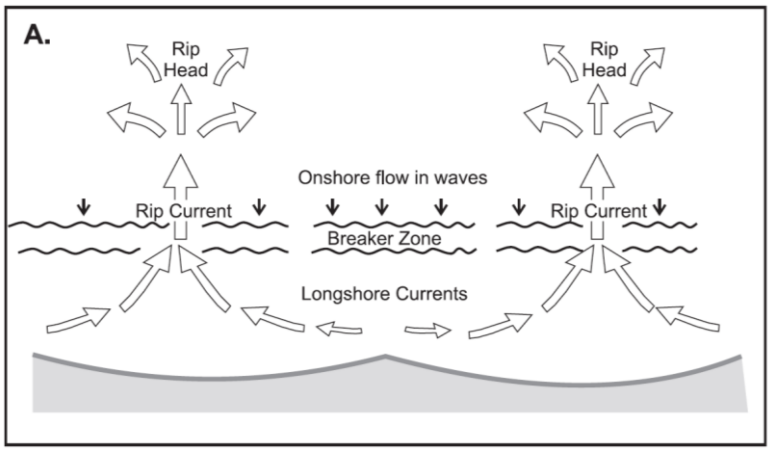

Figure 2.2: Plan view of a rip cell circulation on an open, planar coast. (Source: Davidson-Arnott, 2010)

If instead the shoreface is mostly uniform, most of the onshore mass transport from wave breaking will be compensated through undertow, which is a weaker flow, resulting in smaller offshore directed transport fluxes, but which can be found everywhere in the surf zone (see Figure 2.3).

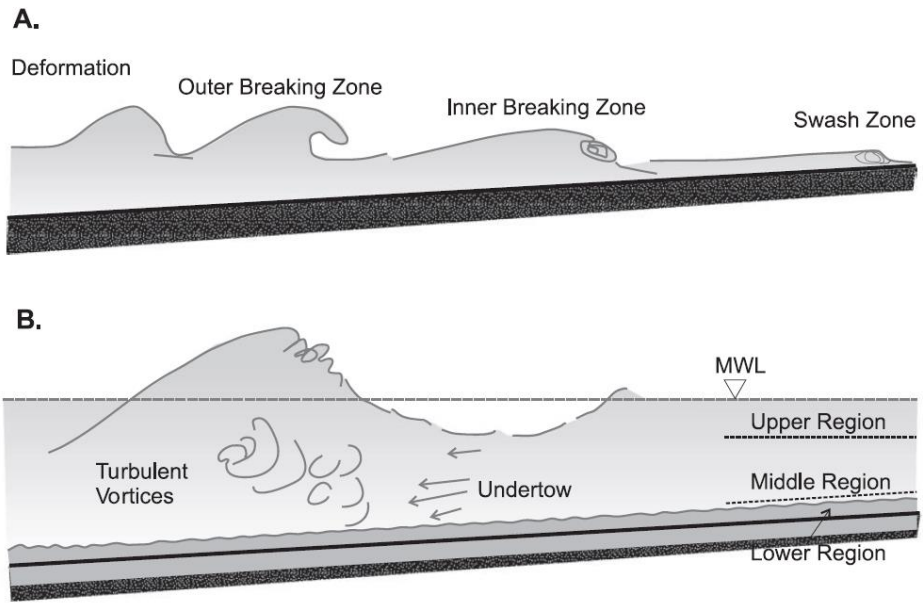

Figure 2.3: Zonation of the surf zone on a simple planar profile: (A) four regions can be identified across the surf zone beginning with the zone of strong wave deformation just before breaking, the area of breaking and rapid transformation in the outer surf zone, the inner surf zone characterised by slowly varying surf bores, and the swash zone where wave run-up occurs; (B) in the outer and inner surf zones the profile can be divided vertically into a region above the wave trough where breaking occurs, a middle zone dominated by turbulence generated by wave breaking and undertow, and a thin boundary layer between the middle zone and the bed. (source: Davidson-Arnott, 2010)

2.2 Findings of previous research

Significant spatial variations in cross-shore suspended sediment transport have been recorded on barred beaches which, unlike the variations on shorefaces of non-barred beaches, do not follow a simple pattern related to increasing depth across the shore (Osborne and greenwood, 1992a/1992b). All of magnitude, relative importance and direction of the individual transport components were found to change depending on the relative position with respect to the longshore bar crests. Onshore-directed incident wave transport was found to increase in landward direction up the lakeward slope, and subsequently decreased on the landward side of the bar crest. This as a result of increased wave energy dissipation on the bar and increased water depths along the landward slope into the trough. Transport induced by both low frequency waves and mean currents were found to increase landward and lakeward of the breaker zone on the bar crest, with consistent offshore directed low frequency wave transport on the lakeward side and potentially shoreward transport on the landward side.
However, these findings came from a lacustrine barred shoreface where tidal influence is essentially non-existent. As such, temporal variance was restricted to mostly wind and wave set-up. Consequently, temporal variance in the relative importance of the transport components were found to only be associated with variability in incident wave energy, specifically during a storm event. The possibility of links between variable relative importance of transport components and other shoreface boundary conditions such as the

shoaling or breaking of waves, presence of surf bores, and various local bed slopes, bedforms and grain sizes, was mentioned but conclusive evidence for this was still lacking.

Aagaard et al. (1998) recorded a period of net onshore suspended sediment transport coincided with onshore bar migration during the first half of an storm event and net offshore transport along with offshore bar migration during the second half. From this they concluded that suspended sediment fluxes measured with velocity and sediment concentration sensors can be qualitatively correlated to topographic changes such as sandbar migration. Onshore bar migration, experienced after the storm had waned, was found to be mainly caused by onshore directed mean transport component. These steady currents were part of a horizontal circulation cell.

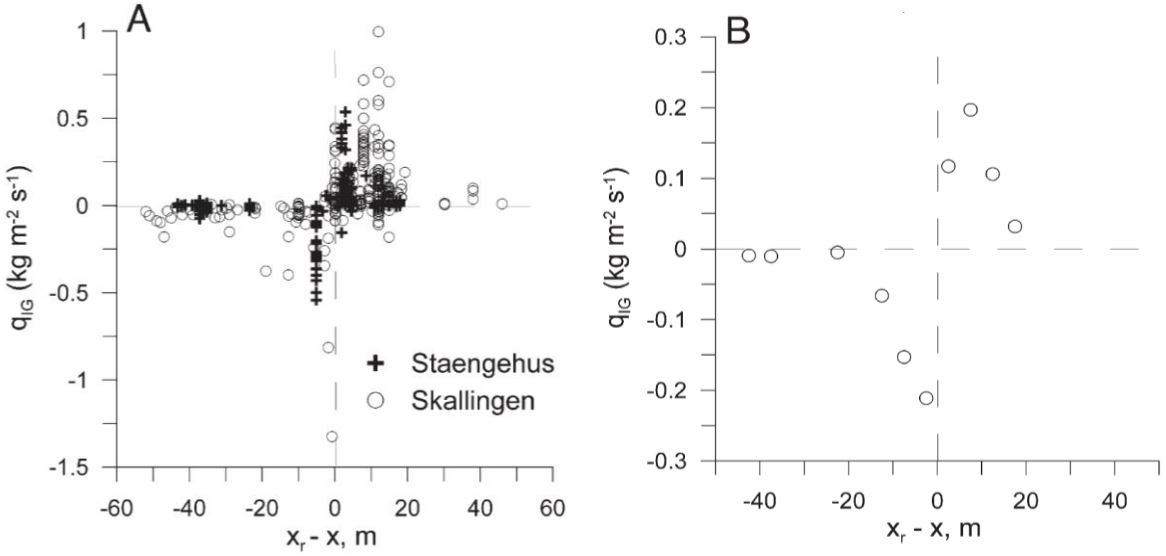

Figure 2.4: A) Observed net IG sediment fluxes (q_{IG}) plotted against measurement position relative to resuspension maxima ($x_r - x$) for all experiments at Skallingen and Staengehus. Positive sediment fluxes signify a net onshore sediment transport and positive values of ($x_r - x$) indicate that the measurement position was located landward of the resuspension maximum; B) Cross-shore IG transport shape function computed from the data in A. The measurements have been aggregated into 5 m cross-shore bins. (source: Aagaard and Greenwood, 2008)

Aagaard and Greenwood (2008) suggested that the direction of infragravity induced transport may be determined by the relative cross-shore position with respect to local relative (incident) wave height maxima at the crests of sandbars, which coincide with resuspension maxima. This idea came forth from the notion that infragravity waves act as an advection mechanism and suspended sand concentrations dwindle slowly in both landward and seaward direction. Their results showed a transport reversal at these resuspension maxima (see Figure 2.4).

Through analysis in the cross-shore variability in the significant of the transport processes for specifically the surf zone of an intermediate state beach, it was found that wind wave frequencies predominantly produce onshore directed transport throughout the entire shoreface, with the exception of the trough between two sandbars where non-breaking waves resulted in small offshore directed transport rates (Aagaard et al., 2013). Sediment fluxes at infragravity frequencies were found to be subordinate to wind/swell wave fluxes. Even in the shallow water (h ~ 0.9 m) above an inner bar of an intermediate state beach incident wave frequencies were dominant over infragravity waves, despite results from a dissipative state beach showing a dominance of infragravity frequencies in comparably shallow waters. Additionally, transport forced by low frequency oscillations were only significant at bar crests, directed offshore at the inner bar crests and onshore at the middle bar.
Relatively small low frequency wave induced transport has also been previously reported by i.a. Ruessink et al. (1998, in the form of bound infragravity waves in the outer surf zone, with negligible contribution from free infragravity waves to the net cross-shore transport) and Conley and Beach (2003, during a storm event); 10-20% on net transport and 20% on net oscillatory transport, respectively.

2.3 Main objectives and research questions

The objectives of this study are to define the relative importance of the three primary transport mechanisms on the cross-shore sediment transport in the shallow, inner surf zone, both (1) temporally and (2) spatially; and (3) relate the mean net transport patterns to (onshore) sandbar migration. Only cross-shore components of flow velocity and suspended sand concentrations, resulting in cross-shore suspended sand transport rates, will be considered in this research; longshore components and bedload transport are omitted.
Based on the literature study it is hypothesized that there is a noticeable difference between (net) transport fluxes during mild or moderate energetic wave conditions and high energetic, storm wave conditions. Furthermore, cross-shore gradients in (net) transport fluxes with respect to sandbars are expected to be present. The transport in the vicinity of sandbars is expected to be net onshore (offshore) directed at times of landward (seaward) sandbar migration. Subsequently, it is hypothesized that nearshore sandbar migration is driven by cross-shore gradients in net transport fluxes.

In light of these aims and hypotheses, the following research questions have been drafted:

1. What is the importance of changing local hydrodynamical conditions (water levels and wave conditions) on the transport components?
2. How does the large scale morphology (position in the cross-shore profile and relative position to the intertidal sandbar) influence cross-shore sand transport?
3. Can (onshore) sandbar migration be explained through sand transport components and what is/are the main factor(s) that importance this process?

3 Methodology

3.1 Relative transport component importance

In order to evaluate the relative importance of the transport components, their individual contributions to the net transport flux are determined in the form of fractions. These normalized flux indices are calculated as follows:

$$Q_{HF} = \frac{\langle q_{inc.HF} \rangle}{|\langle q_{inc.HF} \rangle| + |\langle q_{inc.LF} \rangle| + |\langle q_{mean} \rangle|} \quad (3)$$

$$Q_{LF} = \frac{\langle q_{inc.LF} \rangle}{|\langle q_{inc.HF} \rangle| + |\langle q_{inc.LF} \rangle| + |\langle q_{mean} \rangle|} \quad (4)$$

$$\bar{Q} = \frac{\langle q_{mean} \rangle}{|\langle q_{inc.HF} \rangle| + |\langle q_{inc.LF} \rangle| + |\langle q_{mean} \rangle|} \quad (5)$$

Here, $\langle q_{inc,HF} \rangle$ and $\langle q_{inc,LF} \rangle$ are the time-averaged magnitudes of suspended sediment fluxes due to oscillatory incident high frequency (sea-swell) and low frequency (infragravity) waves, respectively, and $\langle q_{mean} \rangle$ is the sediment flux due to mean (steady) currents. $|\quad|$ denotes the absolute value operator. The sign of the resulting normalized flux indices denotes the direction in which the sand was transported, with negative values representing offshore transport.

In a similar fashion, an index for net transport is used to help reduce the uncertainties in the datasets when comparing data with spatial and temporal differences. This index is the normalized sediment flux index (Q_d) introduced by Aagaard et al. (2002) which, as it is used in this report, is defined as:

$$Q_d = \frac{\langle q_{inc,HF} \rangle + \langle q_{inc,LF} \rangle + \langle q_{mean} \rangle}{|\langle q_{inc,HF} \rangle| + |\langle q_{inc,LF} \rangle| + |\langle q_{mean} \rangle|} \quad (6)$$

Note that infragravity component is included while Aagaard et al. (2002) initially excluded the infragravity component in their calculation of the expression.

Additionally, a variation on a non-dimensional parameter (D), which was found to be a decent parameter for determining the balance between transport fluxes driven by incident waves and those by undertow (Aagaard et al., 2002), will be used in an attempt to determine which hydrodynamical aspects are of greatest influence on the relative importance and directions of the transport components. This non-dimensional parameter is for this report defined as:

$$D = \frac{\sqrt{Sk^2 + As^2} * U_{rms}}{|\bar{U}|} \quad (7)$$

with orbital velocity skewness (Sk) and orbital velocity asymmetry (As), U_{rms} as incident wave (root-mean-square) orbital velocity and $\bar{U}$ as the speed of the undertow.

3.2 Field campaign

3.2.1 Experimental site

The field campaign took place in the shallow surf zone of Vejers Beach, located at the Danish North Sea coast north-east of Blåvandshuk Fyr. The campaign was carried out over a period of 23 days, starting on 18th of September 2016 and lasting till 10th of October 2016. Scheduling the research in autumn (carried over from the summer at 22 September for the northern hemisphere) was a conscious decision; the research project was aimed at analysing the workings of sand transport processes under specifically low to moderate energetic wave conditions and the consensus is that the wave climate during the summer and autumn is generally quite mild energetic. The resulting summer profile of Vejers beach, due to its complex profile characterized by sandbars located within the surf zone, is expected to induce large spatial gradients in hydrodynamic processes (Aagaard et al., 2013). These gradients may produce spatial differences in the relative importance of the transport mechanisms which, when analysed, are expected to give insight in the processes behind onshore sand transport and sandbar migration.

Vejers beach can be characterized as a Longshore Bar and Trough, following the classification model of Wright and Short (1984). The mean slope of the upper shoreface (area of shore shallower than the wave base) is reported as β = 0.006 (Aagaard, 2011), while the foreshore (area of shore between average high tide and average low tide marks) is generally quite steep with a mean slope of $\beta \approx 0.026$ (Jensen et al., 2009).

Either three or four longshore bars are present, which are described as being generally large with steep seaward and landward slopes (e.g. Aagaard et al., 2010, Aagaard et al., 2013). As a result of the rather steep shoreface bathymetry the most common type of wave breaking on the bars is plunging, especially for long-period swell waves. The relief between the bars and relatively deep troughs can be up to 3 m, allowing waves to reform and reshoal after breaking in the shallows waters above the bar crest (Aagaard, 2011).

Mean grain size in the foreshore has been reported as 230 μm (Jensen et al., 2009), while Aagaard (2011) reported grain sizes ranging from $d \approx 0.52$ mm at the crest of the outmost bar and $d \approx 0.12$ mm on the lower shoreface (seaward of the bars). Average mean grain size on the upper shoreface was $d \approx 0.18$ mm, as was the case for the foreshore and inner-surf zone in the spring of 2006. Results of our own grain size analysis, from multiple locations near instruments within the research area, ranged on average between 200 to 230 μm.

3.2.2 Environmental conditions

Westerly winds, recorded from the period of 1995-2007 at Blaavand Lighthouse, are found to be dominant in terms of both speed and frequency of occurrence in the Vejers area, followed by winds from the southwest**.**

The mean annual offshore significant wave height ($H_{s,0}$) is 1.3 m with an average zero-crossing wave period (T_z) of 4.3 seconds (maximum $H_{s,0}$ up to 7 m with T_z of 8.0 seconds), measured by a directional Waverider buoy in ~ 16 m deep water offshore at Nymindegab over the period of 2004-2007. Although south-westerly winds are found to be the second most dominant waves in the area, these are unable to generate strong waves due to the sheltering effects of Horns Rev shoal offshore of Blåvandshuk Fyr on Vejers beach. As such, waves from the northwest are dominant in both magnitude and frequency. From the northwest a low ($H_{s,0}$ < 1 m), quasi-persistent background swell is present. The area has a micro-tidal, semi-diurnal tide, with 1.2 m mean spring tidal range (Aagaard, 2011). The neap tidal range is said to be approximately 0.6 m (Jensen et al., 2009).

3.2.3 Experimental setup and Procedures

Three frames equipped with various measurement instruments were placed in the intertidal zone. The frames, two small transport rigs and a larger turbulence and bedform rig, were positioned in a transect normal to the shoreline and were termed miniframe 15, miniframe 13 and CRD in order of increasing distance to the shoreline, respectively (see Figure 3.1). The two miniframes were both equipped with an electromagnetic field (EMF) sensor to measure flow speeds, a pressure transducer (PT) to measure sea surface elevations and wave heights and three optical backscatter sensors (OBS) used to measure suspended sand concentrations. The single larger frame, referred to as CRD or Truc Vert frame (in reference to the initial deployment of this experimental rig setup during the ECORS Truc Vert experiment, Sénéchal and Ardhuin, 2008) was equipped with three acoustic doppler velocimeters (ADV), a PT sensor, seven seapoint turbidity meters (STM, of which five were mounted vertically to form a vertical array) for measuring flow speeds, sea surface elevations and wave heights and suspended sand concentrations, respectively. Additionally, a 3D sonar intended to observe small scale morphological features such as bed ripples was mounted on the CRD. Some results on the development of the small scale morphology throughout the field campaign are presented in Brinkkemper et al. (2017). Aside from the instruments attached to the frames the research project also made use of ten pressure gauges (OSSI, Ocean Sensor Systems Inc.), five of which were set up alternatingly with the frames along the same cross-shore transect while the other half were placed in a longshore line in the shallow surf zone, covering a total length of 400 m of shoreline in the vicinity of the frames. These additional pressure sensors were specifically deployed to analyse cross-shore and longshore variability in the hydrodynamical conditions, respectively. Results of the alongshore positioned sensors can be found in Naus (2017).

Figure 3.1: Photograph of the setup of some of the instruments deployed in the transect. Taken during high water in the morning of 23th of September during moderate energetic wave conditions. From left to right: OSSI 5, miniframe 15, OSSI 4, miniframe 13, OSSI 3 and CRD. OSSI 2 and OSSI 1, also part of this frame transect, are completely inundated and thus not visible in this photo.

The height of every instrument with respect to the bed elevation was recorded daily during low tide for the duration of the field campaign. Disturbance in the local bed elevation through the contingent presence of scour holes or bed ripples were not carried over in these height measurements.

Local accretion, erosion and/or sandbar migration resulted in dynamic bed elevation throughout the campaign, even on single tidal cycle timescales. Thus often daily adjustments had to be made to keep sensors within the preferred elevation range (within 0.10 m above the bed) while, when possible, taking into account expected bed elevation changes through projected wave conditions for the following tides. Before and after adjustment the height of instruments were recorded. Following this time series of instrument height elevations with 30 minute interval was made to match the time series of data resulting from the data analysis process using linear interpolation.

By daily adjusting the height of the sensors on the frames, to match the change of bed elevation experienced as a result of sand transport and sandbar migration, an attempt was made to keep the sensor elevations consistent with respect to the bed throughout the field campaign. The EMFs of miniframe 15 and 13 were kept at elevation between 0.10 and 0.25 m above the bed along with three OBSs, placed vertically with one at equal elevation and the other two at -0.05 and -0.10 m relative to the EMF.

The contributions of the transport flux due to mean currents (referred to as the steady component) were determined by multiplying the mean flow velocity and mean suspended sand concentration of the 30 minute sections. Oscillatory flows were separated at 0.05 Hz into high frequency and low frequency oscillations. Excerpts of the velocity and concentration

data for the three components with the resulting transport components are shown in Figure 3.2. No attempt has been made to separate the oscillatory flows in those due to incident waves and those due to reflected waves, nor the effect of bound infragravity waves from free ones.

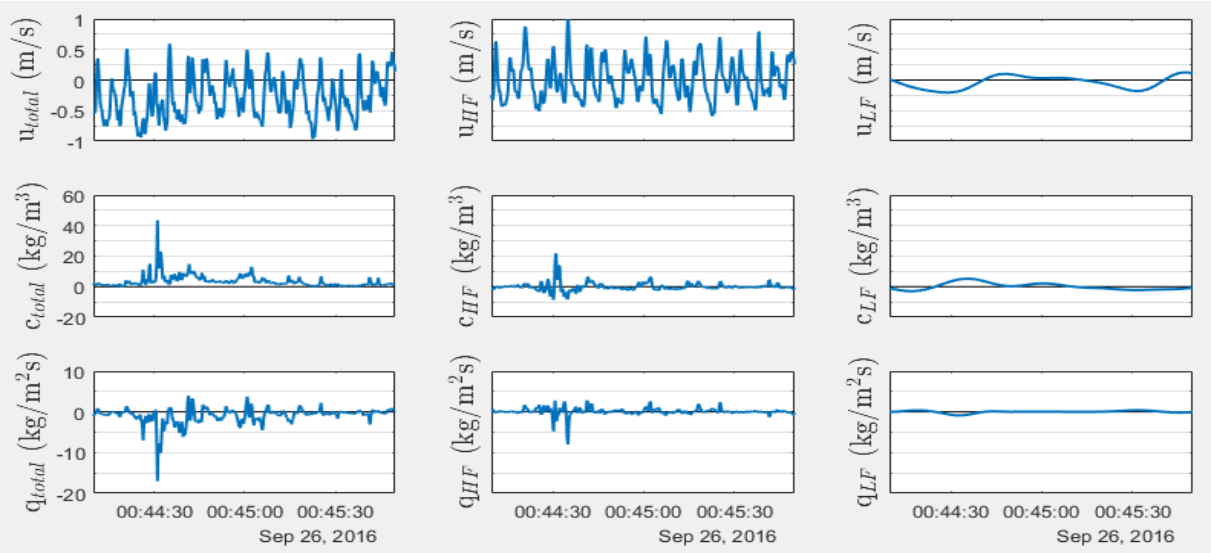

Figure 3.2: Two minute excerpts of the net velocity, concentration and resulting transport time series and corresponding time series of the high frequency and low frequency components.

Part of the field campaign included surveying morphological changes across the beach and nearshore bed of Vejers beach, covering an alongshore area of 400 m of beach and shoreface. The RTK-GPS was attached to a wheel and was walked along cross-shore rows with 10 to 20 m spacing, daily collecting between 3000 and 7500 data points with 1 Hz sampling rate. The cross-shore bed elevation profiles comprised of data gathered in the row closest to the frame transect are used in this report.
Since the wheel necessary for this setup arrived at the 26th of September, the measurements during the first week of the campaign had to be carried out by moving the RTK-GPS by hand and manually activating it to record each point. Naturally this process takes more time and as such far less points could be recorded. The resulting height elevation maps and cross-shore profiles for the first week were therefore significantly less detailed.

Lastly, daily 10 minutes time exposure (timex) images were taken with a GoPro camera during high water. The GoPro was positioned on of the dune ridge, about 12 m higher than the beach front, close to the transect of the frames to get an overview of the survey area. After removing the distortion (fisheye) effect, the resulting images were used to picture the longshore variability and position of the (subtidal) sandbars.

3.3 Data Processing and Selection

The concentration time series measured by the three OBSs for miniframes 15 and 13 and seven STM's of CRD were screened in order to identify moments at which the sensors had been (negatively) affected by factors other than the suspended sand concentration and thus produced incorrect data. This screening process was the same for all raw data time series and consisted of the steps described in this section.

Initially, all time series were split in sections of 30 minutes, matching the windows at which the data would be analysed afterwards. Following the screening process either adjustments would be carried out to correct faulty raw data within a section or the section of raw data would be excluded from the data analysis altogether. The instrument height time series were used to check the estimated OBS or STM instrument height for each 30 min section of data. The choice was made to preferably use data for which the instruments were positioned in the lower part of the water column, between 0.01 and 0.10 m above bed elevation. Instruments positioned lower can create scour holes which disturb the water flow and suspended sand concentration through increased turbulence resulting in unreasonably high or unreliable data. Adversely, instruments positioned at high elevation above the bed may record only low concentrations as the sand may not be suspended as far up the water column, especially under low energetic wave conditions.

Afterwards a number of checks were applied on each 30 min section of the concentration time series separately. First sections with an unexpectedly high average sand concentration, thought to be either influenced by a large amount of bubbles in the water (which are mistaken by the OBS and STM as suspended sand particles), sea weed wrapped around the instruments, or sections during which the sensors were partly buried in the sand bed. Additionally section with unreasonably high peaks, also thought to be influenced by bubbles, were excluded. Examples are shown in Figure 3.3.

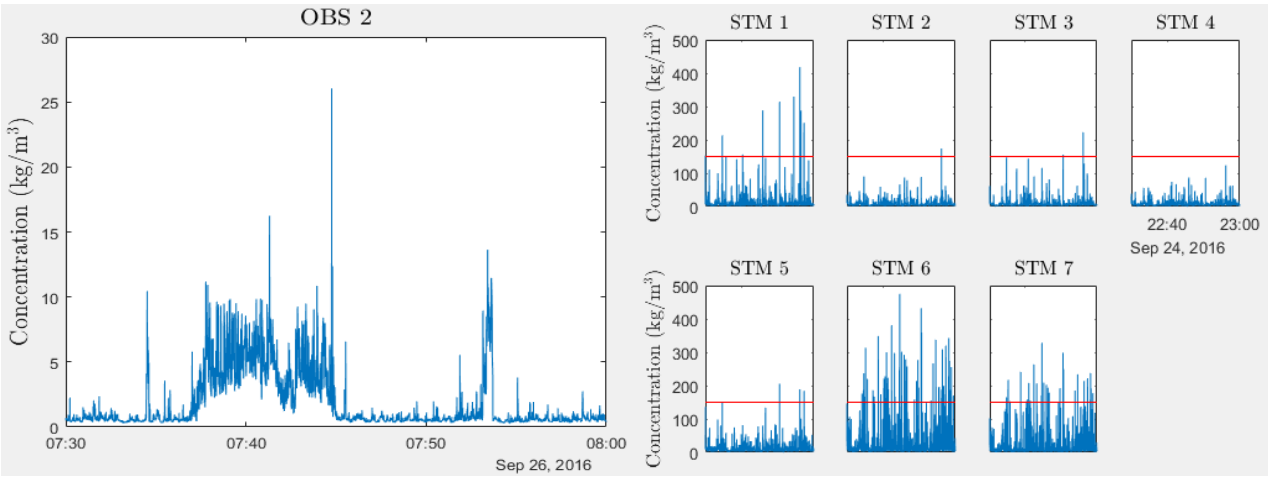

Figure 3.3: On the left an example of what is deemed to be unsuitable concentration data, possibly as a result of sea weed in the view of OBS 2 of miniframe 13. On the right the time series of all seven STM's of the CRD of which all but one were excluded from analysis as a result of having moments where the concentration fell above the threshold which was set to 180 kg/m^3 (indicated by the red line).

Next the data was manually screened, going through each section to visually identify any additional unconformities which were not picked up by the previous steps of the screening process. Example of a section with such 'faulty' data is shown in Figure 3.4.

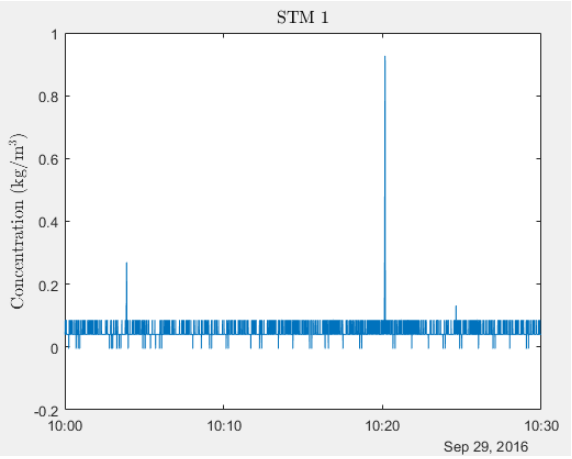

Figure 3.4: Section identified as consisting of faulty concentration data, consequently excluded from the data analyses process.

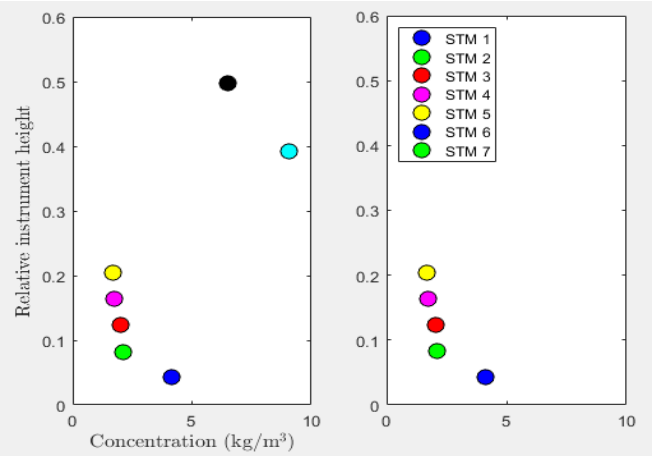

Figure 3.5: Vertical concentration profiles for a section before (left) and after (right) removing data from instruments which resulted in an inverted profile. The points in the profiles are the mean concentrations of the seven STM sensors deployed on the CRD frame.

Lastly the data was screened for inverted concentration profiles (see Figure 3.5). Since it is recognized that it is possible for suspended sand concentration to temporarily be larger for higher elevations in the water column than at a lower elevation, the mean concentrations over 30 min sections were used. By comparing the mean value between instruments with different elevations on the same frame, sections of data from an instruments positioned at a higher elevation but which nevertheless recorded higher mean concentration could be identified and excluded from analysis. Such high concentrations would be either due to bubbles in the water or sensors (partly and temporarily) covered by seaweed.

Additionally, a condition for the data analysis process was set that the calculations would only be carried out for sections for which data was available for the entire duration of 30 minutes (7200 data points at a 4 Hz sampling rate). Since the ADVs deployed on the CRD take one minute in each 30 minute section to prepare itself for measurements, this requirement was set to 29 minutes for the relevant datasets.
OBS and STM sensors were calibrated by using sand samples from the field in a recirculation tank, fitting a 2nd order polynomial through the sensor response data points for 0-20 kg/m^3 sand concentration range. Slight deviations between the calibration curve and actual sand concentration exist, particularly for lower concentrations. These deviations may result in a certain background concentration in the data gathered in the field along with the possible presence of turbid water due to significant portion of particles finer than sand suspended in the water. In an attempt to eliminate this background concentration the third percentile concentration was calculated for each section of data separately and subsequently removed.

A finalized time series consisting of data composite from different OBSs or STMs of the same frame was made as part of the data analysis process. The dataset of the lowest positioned sensor would be used and, where possible, filled in with data from higher positioned sensors whenever there was initially no data available. By merging the individual datasets of the different concentration sensors on a single frame, a most complete concentration time series is constructed. These composite datasets were used as the finalized concentration time series in the calculations and results on sand transport fluxes in this report.

Tables 1-3: Total number of data points left after each step of the screening process for each of the frames. Data was collected at 4 Hz sampling frequency. Only the composite datasets are used in the calculations for the results in this report.

CRD		Screening					Result
	Unfiltered data	High values	High average	Unconformities	Inverted profile	Analysed data	Composite dataset
C1	4687200	2080800	1425600	1036800	799200	741600	1706400
C2	4687200	2606400	1929600	1634400	1461600	1245600	
C3	4687200	2318400	1555200	1360800	518400	468000	
C4	4687200	2217600	1605600	1332000	626400	489600	
C5	4687200	2023200	1468800	1296000	252000	223200	
C6	4687200	1159200	1094400	964800	432000	388800	
C7	4687200	1483200	1468800	1144800	756000	720000	

Miniframe 13		Screening					Result
	Unfiltered data	High values	High average	Unconformities	Inverted profile	Analysed data	Composite dataset
C1	3196800	2836800	2674800	2505600	874800	633600	2275200
C2	3196800	2811600	2725200	2462400	2397600	2102400	
C3	3196800	2448000	2390400	2070000	1418400	1382400	

Miniframe 15		Screening					Result
	Unfiltered data	High values	High average	Unconformities	Inverted profile	Analysed data	Composite dataset
C1	2455200	2152800	1857600	1756800	705600	439200	1612800
C2	2455200	1836000	1728000	1519200	1501200	1353600	
C3	2455200	1958400	1933200	1764000	954000	784800	

Sections for which the instrument was positioned below the bed elevation, and as such was expected to be buried under the sand, positioned in a scour hole or rather close to the bed, were initially excluded from the data analysis process. Additionally, sections of data for which the instrument was positioned higher than 0.1 m above the bed were excluded as well. However, it was found that a significant amount of valuable data, otherwise deemed suitable for data analysis if not for a disqualification on the basis of its corresponding interpolated instrument height, was left unused.
It was recognized that the interpolated time series of instrument heights is rather unreliable, especially for moments in time that local bed elevation changed rapidly as a result of bar migration. Consequently, rather than taking the linearly interpolated instrument height time series at face value and subsequently excluding data on this criterion alone, extra notice was taken of the fitness of data in the sections that failed the instrument height criterion but are otherwise not eliminated by the screening process. If this data was still deemed suitable it was retroactively included in the data analysis. Tables 1-3 display the number of concentration data points left after each step of the screening process, along with the finalized composite dataset, for each of the frames.
After this data screening and selection process, the cross-shore flow velocity (u) time series measured by an EMF or ADV were coupled with the composite suspended sand concentration (c) time series, measured by the OBSs or STMs, to calculate the net cross-shore sand fluxes. Both flow velocity and suspended sand concentration were additionally dissected into components of mean currents and oscillatory flows (high frequency and low frequency signals separately), as shown in the literature study.

3.4 Categorization

While the research project was launched with the intention of analysing sand transport during moderate energetic wave conditions, three periods of highly different wave conditions were met throughout the field campaign, which can be recognized in both wave data from an offshore wave buoy (see Figure 3.6) and OSSI 1 (which was the most seaward positioned pressure sensor along the frame transect, around 50-60 m and 75-95 m offshore from the high water level shoreline before and during the storm, respectively, in ~ 1.5-2.0 m deep water). From these wave condition time series combined with the morphological data shown in Figure 3.8 four different categories had been identified. Firstly periods of onshore sandbar migration were separated from periods of offshore migration. Secondly, further distinction was made on the basis of difference in offshore wave height and period. All data time series gathered during the field campaign were subsequently split in accordance with these categories.

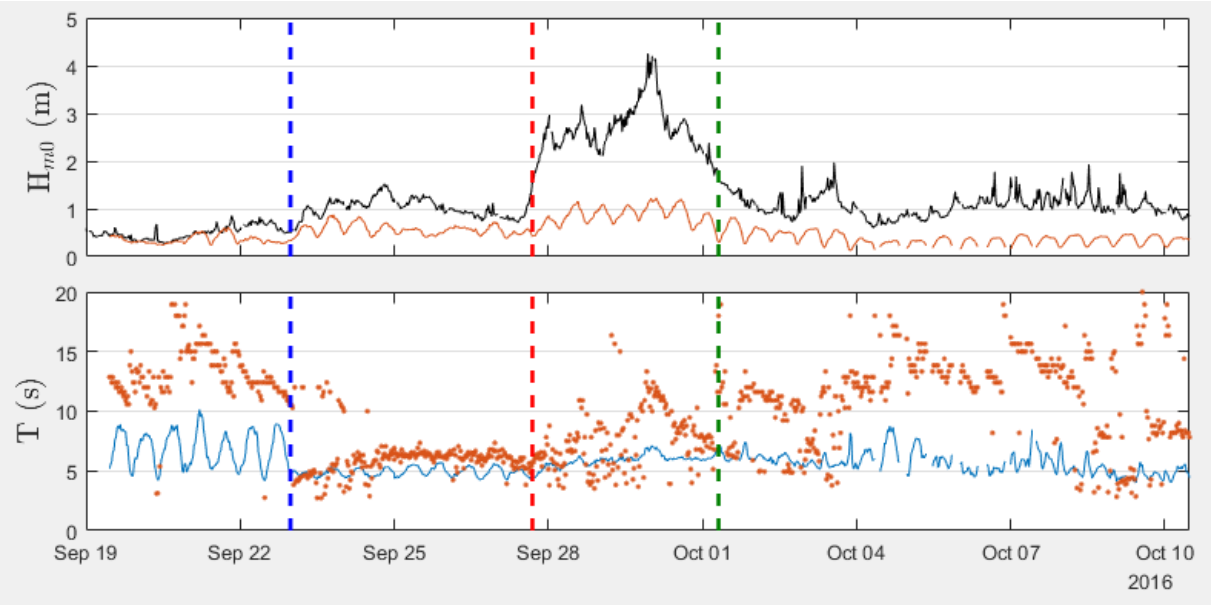

Figure 3.6: Depiction of some of the wave conditions experienced throughout the field campaign and the categorization of the data that was derived from it, visualized with vertical dashed lines. Top plot shows the offshore wave height in black and local m_{01} wave height (OSSI 1) in orange, taken from an offshore buoy in ~ 16 m deep water. Bottom plot shows the local peak wave period in orange and m_{01} wave period in blue.

The resulting number of half-hour averaged transport data points available within each category per frame are shown in table 4.

Table 4: Number of transport data points available for the three frames for each of the four categories after the screening process.

	Category 1	Category 2	Category 3	Category 4
CRD	237600	280800	712800	475200
Mini 13	122400	748800	1072800	331200
Mini 15	43200	410400	964800	194400

3.4.1 Wave conditions

During the first few days of the field campaign, from 18 till the end of 22 September, wave conditions were characterized by low, long period swell; median offshore wave height of 0.5 m (0.28-0.86 m range), local height of 0.33 m at OSSI 1 (0.23-0.62 m range), median Tm_{01} of 6.9 seconds, median Tpeak of 12.9 seconds. Supposedly, before our arrival and start of the field campaign Vejers beach had already been subject to similar conditions for approximately a week. These low energetic conditions are ascribed to easterly winds which blow in offshore direction for the north-west facing coastline, resulting in the subordinance of wind waves in the sea state.

At the end of the 22th of September the winds turned from easterly to west/south-westerly. This resulted in much different wave conditions; larger waves (1.02 m median, 0.54-1.56 m range, offshore and 0.56 m, 0.34-0.87 range, locally) with a significantly shorter period (median Tm_{01} of 4.9 seconds and Tpeak of 6.1) during the second category (start of 23 till

midday of 27 September). Through wave counting in the field during high water in the early morning of 23 September it was estimated that around 2/5th of all incoming significant waves broke near CRD. Counting was repeated near the end of this category at the end of the morning on 26 September. Now only 1/5th of the waves broke near CRD while 2/5th broke near miniframe 13.

The third category, lasting from midday 27th of September till early 1st of October, is characterized by a storm which brought high energetic wave conditions in the form of significantly higher waves; offshore median height of 2.61 m (1.56-4.26 m range), local height of 0.87 (0.30-1.23 m range) with 6.0 second Tm_{01} and 7.7 second Tpeak.

During the fourth and last category the waves returned to similar long-period swell conditions as were experienced during category 1, though with higher wave heights. Offshore median height was 1.07 m (0.61-2.38 range), local height of 0.38 m (0.13-0.82 range), and Tm_{01} period of 5.6 seconds with a peak period of 12,0 seconds. Wave counting in the afternoon of 2nd of October revealed that 2/7th of the waves broke near CRD and just over half near miniframe 13. Later in the category, in the afternoon of 4 October, 1/5th of waves broke at CRD.

Subtracting the projected high and low tide sea surface elevations from the actual sea surface elevations measured during the field campaign (recorded with OSSI 3) shows the deviations in local water levels as a result of wind direction and low-/high-pressure areas near Vejers beach (see Figure 3.7). The significant levels of negative storm surge visible during the first and second half of the last category are attributed to the prevailing offshore directed winds during these periods. Additionally, limited relative water levels during the second and last category were in part due to neap tides.

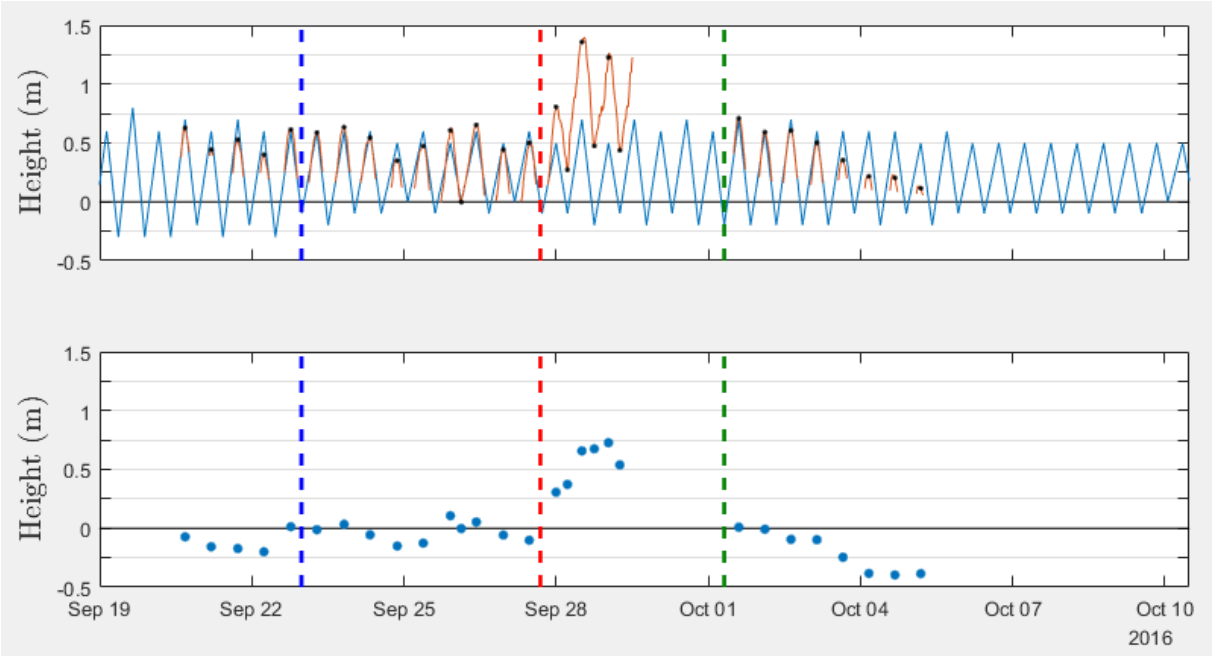

Figure 3.7: Projected tidal sea surface elevations at high and low tide for Hvide Sande (blue solid line) and time series of the sea surface elevation levels measured by OSSI 3 (red solid line) in the top plot, and the difference between the two displayed in the bottom plot. The difference gives an indication of the amount of (storm) surge throughout the categories. Tidal data was taken from an online Danish Meteorological Institue (DMI) database. The data was adjusted to estimate projections for Vejers beach.

3.4.2 Morphological change

Cross-shore profiles

The research area was surveyed once every single day during low water with a RTK-GPS. Resulting cross-shore profiles near the frame transect are shown in Figure 3.8.

As mentioned earlier, Vejers beach was exposed to long period swell waves for almost two weeks, of which the last five days took place at the beginning of the field campaign. Cross-shore profiles from these last five days show a alternation of landward and seaward migration of the intertidal sandbar at a variety of rates (maximum of ~ 5 m/day landward), being moved ~ 5 m further shoreward than at the start of the field campaign. At the end of the first category this sandbar had moved far enough up the profile that it became partly attached to the upper beach. Due to the high elevation of the bar crest and the relatively low water elevations the sandbar was no longer being fully inundated, even at moment of maximum high water. Now, only occasional waves reached high enough to overtop the bar. The overwash would flow towards the lowest elevated parts of the trough between the sandbar and beach where it would collect in puddles (see bottom right of Figure 3.9a).

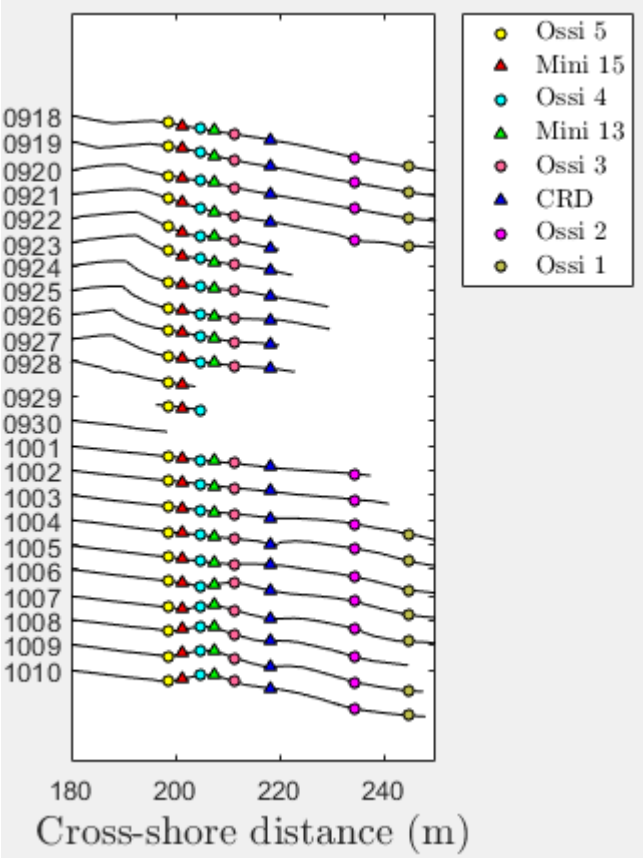

Figure 3.8: Evolution of the bed profile throughout the field campaign. Position of the instruments deployed along the profile are indicated with the markers. The x-axis represents the distance to a reference point in the dunes.

During the moderate energetic conditions in category 2 the sandbar remained relatively stable in its cross-shore position, migrating at a maximum pace of ~ 2 m/day and being moved ~ 2.5 m in landward direction over a four day period, as migration of the sandbar was mostly halted due to a lack of inundation. Instead, morphological change now came predominantly in the form of steepening of the seaward facing slope (up to 15°), which took place as a result of wave runup. A portion of this reworked sand of the seaward facing slope was subsequently distributed over the shoreface, reducing the slope of the seabed between the instruments (from ~4.5° during category 1 to < 3.6° during category 2).

The storm that followed afterwards (category 3) quickly removed the sandbar from the beach, spreading its sand throughout the inner surf zone while simultaneously straightening the beach profile while further lowering its slope (< 2.4°). Profile data were lacking for most of

the storm event due to the unfavourable weather conditions (unable operate the RTK-GPS during rain) and high water levels, even at low tide, making it impossible to measure along the deeper portions of the frame transect.

The return to low/moderate conditions during category 4 in the wake of the storm allowed the beach to recover. At 3 October the first signs are visible of the intertidal bar re-entering the transect profile between CRD and OSSI 2. This moderately low sloping (~ 6.0°) sandbar subsequently migrated onshore (net landward movement of ~ 16 m in 4 days, maximum migration rate of ~ 8.5 m/day) till it became more or less stable and steepened (> 7.7°) from 7 October onwards for the remainder of the field campaign. The cause was much similar to the one found for category 2; low water levels prevented inundation and limited sand transport to overwash during (maximum) high water. Meanwhile, a second intertidal bar emerged in the transect profile around 6 October between CRD and OSSI 2 which proceeded to migrate in landward direction (~ 5.5 m net movement, ~ 3 m/day maximum rate).

Longshore variability

Figure 3.9 shows time-exposure images overlooking most of the research area, with the frame transect positioned just around the middle. The images were taken during low water at various moments throughout the field campaign and illustrate the development of the position and longshore variability of the intertidal and/or subtidal sandbar(s) through wave breaking patterns. Indication of the position and longshore variability of the swash bar and shoreline can also be gathered in the images through colour differences in the

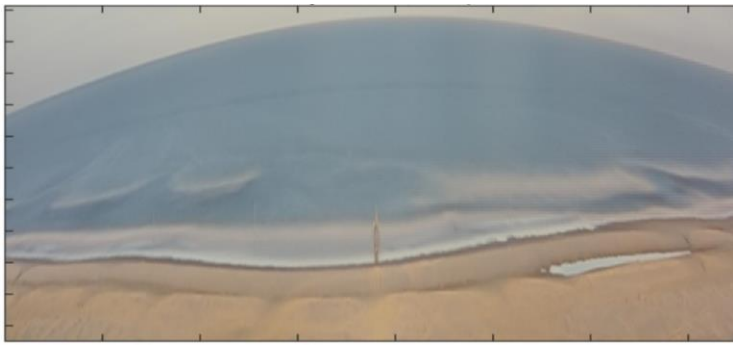

a) 27 September 2016, 08:00

b) 30 September 2016, 10:05

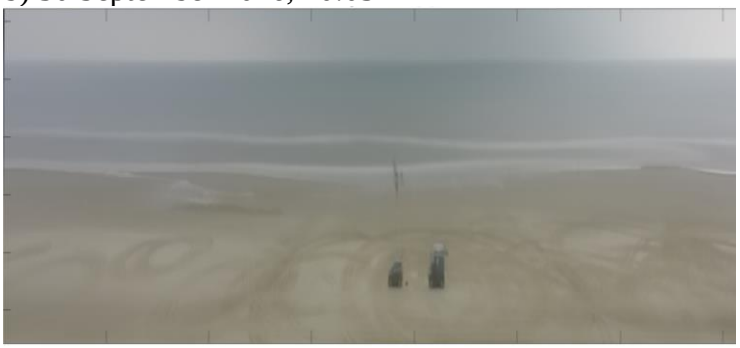

c) 2 October 2016, 09:30

d) 10 October 2016, 12:45

Figure 3.9: Timex images of the survey area during low water taken just before the storm (a), during the storm event (b), directly after the storm event (c), and at the end of the field campaign. On images b, c and d correction for the fisheye-effect has been applied.

sand, though these are less pronounced. Figure 3.9a was taken near the end of category 2, just before the storm, when the inner intertidal sandbar tracked with the cross-shore profiles from Figure 3.8 had reached its most landward position as it had partly welded to the upper beach. The trough between sandbar and beach can be seen through the darker colour of the sand and water trapped within it is visible on the right hand side. A total of three sandbars, of which two subtidal ones, are all shown to be positioned within a few hundred meters of the beach, and the subtidal bar is revealed to be highly crescentic, despite the sandbars being generally described as straight in the literature. These aspects are indicative of the long lasting low and moderate energetic conditions that came before and which have led to onshore migration and significant longshore variability. The sandbars appear straighter in Figure 3.9c than they were in Figure 3.9a, only a couple of days before. The last image (Figure 3.9d) shows the resulting beach and nearshore morphology after an additional week of low to moderate energetic wave conditions throughout category 4 which encompassed a return to low energetic, long period swell waves. The intertidal sandbar which has again been migrating in the landward direction and pushed up the shoreface is faintly visible around the height of the frames shown in the centre of the image. Once more two subtidal bars can be seen in the image. Noteworthy is the lack of significant longshore variability present in these subtidal bars despite the similar hydrodynamic conditions experienced throughout category 1 and 2. This suggests that the return of longshore variability takes more time than the ~ 10 day duration of category 4.

4 Results

4.1 Temporal change in hydrodynamics and transport

4.1.1 Categorization

First, the different hydrodynamical conditions for each category will be further examined (see Figure 4.1). Only the data and results gathered by the CRD frame are used in this section of the report; this frame has gathered the longest continuous sections of data due to its further offshore and lower elevated position, making it the most suitable frame for analysis of the effects of tidal cycles on the recorded transport rates. Furthermore, by focusing on a single frame rather than combining the data of the three frames, effects of the different cross-shore positions of the three frames on the results will not be factor that has to be accounted for in the interpretation of these results. This dependency (cross-shore variability of hydrodynamics and resulting transport) will be discussed separately in section 4.2 of this report.
It is worth mentioning that although the field campaign lasted till 10 October, at which the frames and OSSIs were removed from the site and the last cross-shore profile was measured in, most of the instrument deployed were unable to gather any or suitable data for a considerable portion of the last category. The significant amounts of negative storm surge experienced during the last days of the field campaign, causing either the frames and OSSIs to not be submerged by water and start measuring or disturbance of the data through bubbles in the data which was subsequently removed through the filtering process, no transport data is available past the 4th of October. Therefore, time series in the figures will be cut off at the moment where the last transport data is available.

In the first category relative wave height occasionally falls below the 0.4 ratio mark, indicating that the then recorded waves were not breaking. The water depth and significant wave height time series show that this is due to the relatively small wave heights (down to ~ 0.25 m, even at peak tide) during these sections. A combination of generally high wave skewness (in the order of 0.75-1.5) and wave asymmetry (1.0-1.7), along with the overall longest wave periods (9.8 s), additionally characterizes category 1. Throughout the rest of the field campaign waves have been continuously breaking. Even for the second half of category 4 during which the wave conditions returned to similar long period swell waves. Despite the low wave height (as small as 0.1 m), even in comparison to the waves from category 1, significantly lower water depths still caused the waves to break.

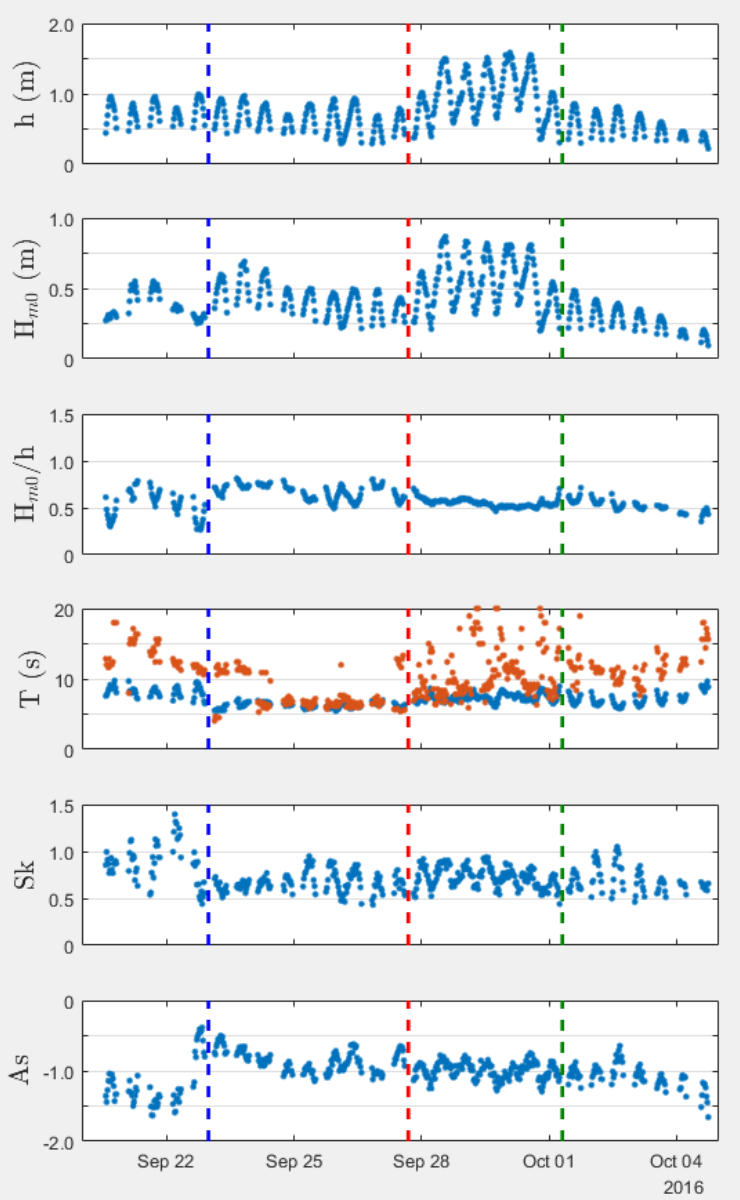

Figure 4.1: Time series of the hydrodynamical conditions. Data taken from the CRD frame.

The water depths for category 2 are comparable with those found in category 1 (ranging from 0.5-1.0 m for mid to high tide), but generally significantly higher waves were recorded at peak tide (> 0.5 m). The resulting relative wave heights for category 2 were generally the highest throughout the campaign, as the significantly higher (storm) waves experienced during category 3 were compensated by further increased water depths. Additionally, the majority of category 2 consists of waves with the generally lowest wave period found throughout the field campaign.

Category 3 is comprised of a storm event. The highest waves and highest water levels, due to the storm surge (see Figure 3.7), at peak tide for the campaign characterize this category. As a result of these high water levels the CRD was positioned outside the intertidal zone, allowing it to record continuously through both high and low tide. This reveals that the waves do experience significant decrease in height for the low tide which is actually on par with the decrease in water depth, resulting in a mostly stable signal of relative wave height throughout the tides of this category. Tidal variation is still recognizable in the signals of wave skewness and asymmetry, which are comparable to the signals in the second half of category 2.

Lastly, category 4 has similar mild energetic wave conditions in its first half as the second half of category 2, while for its second half a return to low period swell waves and quite extreme low water levels, akin to category 1, is experienced. While the values for wave asymmetry for this second half are appropriately similar to those found during category 1, skewness is generally much lower (ranging between 0.5-0.7). This may be due to the lower local water depths, which tends to reduce wave skewness.

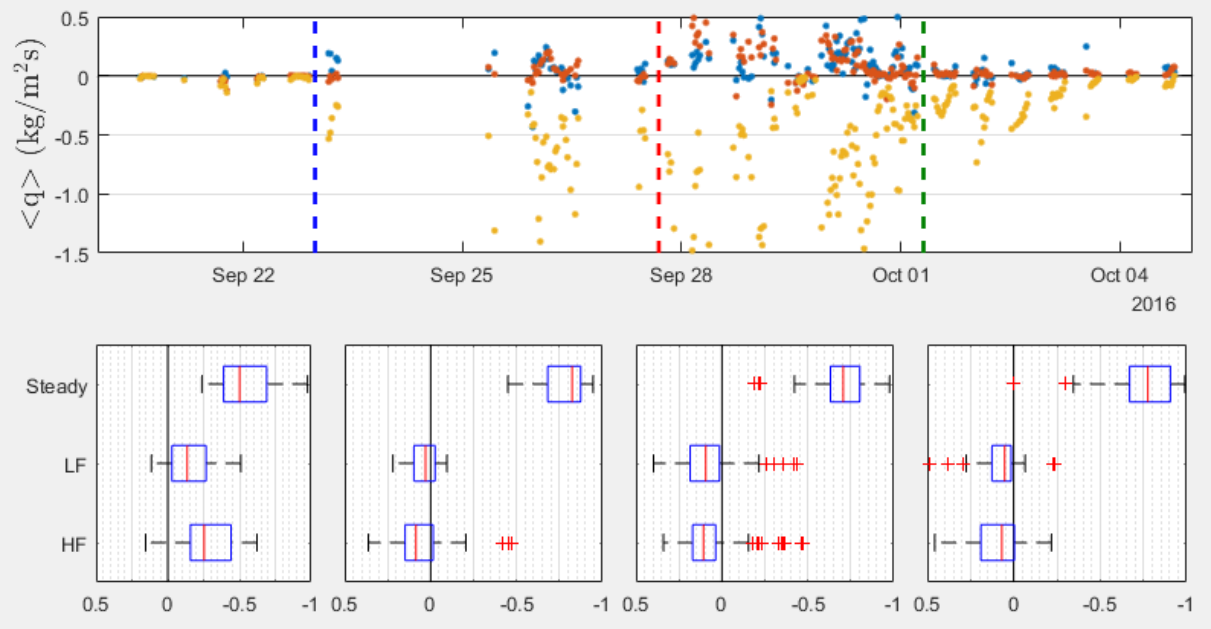

Figure 4.2: Top plot: transport components; HF in blue, LF in red, steady component in yellow. Bottom plots: boxplot per category; median by the vertical red line, the right and left hand edges of the blue box as 25th and 75th percentile, respectively, and extreme data points with the whiskers and outliers through red crosses. Positive values denote onshore directed currents and transport fluxes.

Figure 4.2 gives an overview of the three transport components (high frequency and low frequency components, abbreviated to HF and LF, respectively, and a steady component) for CRD throughout the four categories, both in magnitude as time series and relative importance in the form of boxplots which result from these hydrodynamical conditions. The boxplots display the transport fraction data for each of the four categories. The gap in the concentration time series in the category 2 from the afternoon of 23 September to 25 September is mostly due to the STM's becoming buried as a result of high rates of local accretion, resulting in unsuitable data that is consequently left out of the data analysis. Time series of the suspended sand concentration and velocity components, measured by the CRD, can be seen in Figure A.1. Additionally, the resulting time series of net transport rates is shown in Figure A.2. Time series of the net transport rates for miniframes 13 and 15 are shown in Figure A.3, though this data will not be discussed in this section of the report.

Net transport is generally largest during category 3; up to 0.5 kg/m^{2}s for HF and LF components, and 1.5 kg/m^{2}s for the steady component, with both relatively high flow velocities (up to 0.5 for HF, 0.3 for LF and 0.4 m/s for steady component) and suspended sand

concentrations (up to 4.5 for HF, 3.7 for LF and 5.4 kg/m^3 for steady) for each of the transport components in comparison to the results of the other three categories (see Figure A.1). Comparably high transport and associated concentrations and flow velocities for the steady component can be seen during the second half of category 2. However, transport of the HF and LF components is here generally significantly smaller (up to 0.25 and 0.2 kg/m^{2}s, respectively), which is predominantly due to lower orbital velocities (up to 0.4 for HF and 0.2 m/s for LF, while concentrations are still comparatively high).
Transport rates during the first and last category were significantly lower (up to 0.04 HF, 0.13 LF and 0.14 kg/m^{2}s steady, for category 1; up to 0.25 HF, 0.08 LF and 0.73 kg/m^{2}s steady, for category 4) with both much smaller velocities (0.45 HF, 0.2 LF and 0.1 m/s steady, category 1; maximum of 0.3 m/s for all three components) and concentrations (1.6 HF, 2.3 LF and 2.6 kg/m^3 steady, category 1;2.4 HF, 3.4 LF and 5.6 kg/m^3 steady, category 4).

Table 5: Values of the 25th, median, and 75th percentiles for the transport component fractions for each of the categories.

	Cat. 1			Cat. 2			Cat. 3			Cat. 4		
	25th %	75th %	Median	25th %	75th %	Median	25th %	75th %	Median	25th %	75th %	Median
Steady	-0.69	-0.39	-0.50	-0.87	-0.68	-0.82	-0.80	-0.63	-0.71	-0.91	-0.67	-0.78
LF	-0.27	-0.03	-0.14	-0.03	0.10	0.03	0.01	0.19	0.09	0.01	0.13	0.05
HF	-0.44	-0.16	-0.25	-0.01	0.15	0.08	0.04	0.17	0.11	0.00	0.19	0.07

The boxplots in Figure 4.2 show the median and range in the transport components for all the data collected for each of the categories. From these plots and table 5 it is noted that for category 1 the relative importance of the steady component was on average much smaller than for the other categories; median of -0.50, while it ranges from -0.68 to -0.78 for the other three categories. This is mostly due to the HF transport component which was significantly larger for category 1 with a median of -0.25, compared to a range of 0.07 to 0.11 for the other categories. Moreover, category 1 is the only category with negative (offshore) median values for either the HF or LF components; categories 2 to 4 all show positive (onshore) median values for both HF and LF components, admittedly with a 25th percentile either close to or just past the zero mark.
Overall, quite comparable transport fractions are shown for categories 2, 3 and 4. This despite the considerable difference in hydrodynamical conditions. A possible explanation may be that for the low to moderate energetic wave conditions of categories 2 and 4 only during the highest parts of the tide transport data was collected, this due to the low relative water levels, while for a portion of the storm event the frame continuously gathered data for days on end during both low and high tide.

While relatively large transport due to oscillatory currents is expected for the categories with low to moderate energetic wave conditions, particularly because of the reduced wave breaking, the direction of the HF and LF components for especially category 1 is predominantly offshore. This goes against the expectations as these components thus only contribute to the offshore directed transport forced by the steady component rather than

working against it. This results in a larger net offshore directed transport flux while the wave conditions for this category were initially deemed to favour onshore net transport.

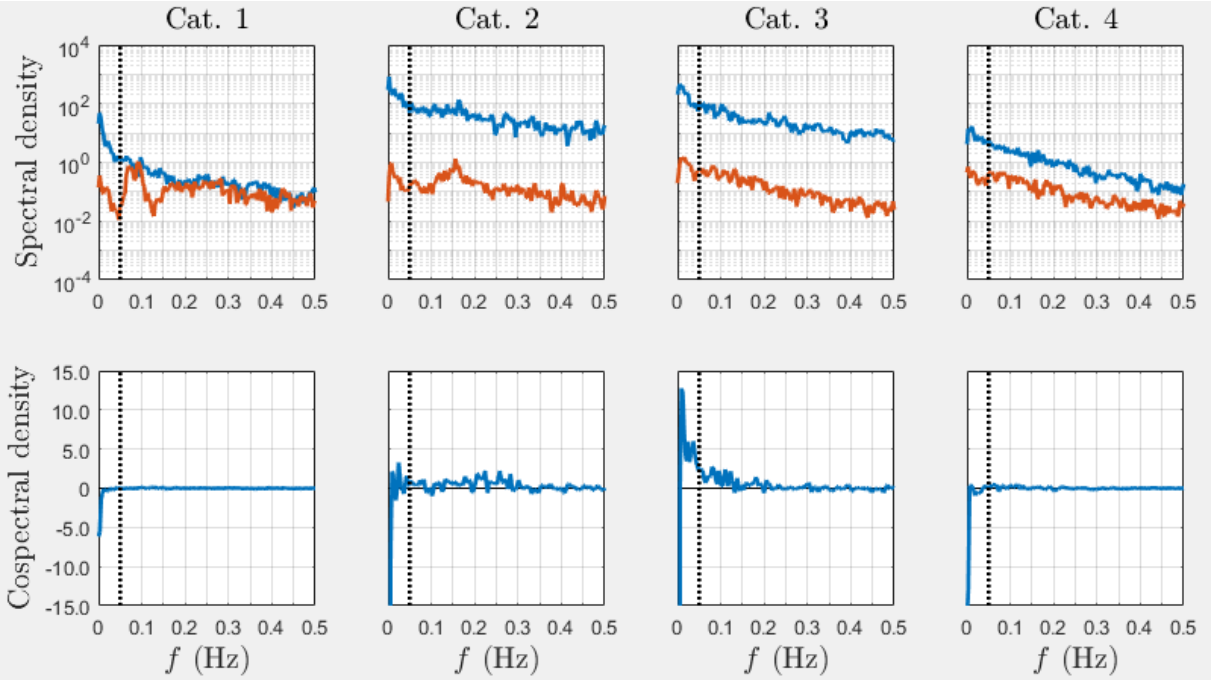

Figure 4.3: Top plots display suspended sand concentration ({kg/m^3}^{2}/Δf, in blue) and cross-shore velocity ({m/s}^{2}/Δf, in red) spectra, recorded at peak high tides for each of the four categories; 22 September, 22:21, 26 September, 01:00, 28 September, 04:30, and 1 October, 17:30, respectively. Bottom plots are the resulting transport cospectra. Positive cospectral values indicate onshore directed transport.

Through spectral analysis similarities and differences between the four categories can be further identified through the predominant frequencies that contributed to the net transport (see Figure 4.3). Spectra of category 1 is characterized by the high peak in cross-shore velocity from the swell waves, between 0.05 and 0.13 Hz (peaking at 0.09 Hz) and low spectral density for suspended sand concentration. Additionally, a broad bulge in cross-shore velocity can be seen for sea waves, between 0.13 and 0.03 Hz. The cospectra partly matches the result from Figure 4.2 by showing very little transport across the spectrum, with on average offshore directed transport in the infragravity band and generally offshore directed wind wave transport. However, relatively large peaks of onshore directed transport can be found for swell waves between 0.10 and 0.14 Hz.

The velocity spectrum of category 2 shows broad peak in the incident wave band at 0.16 Hz, ranging from 0.10 to 0.24 Hz. Significantly higher spectral density can be seen for concentration, comparable with the spectrum of category 3, than category 1. This was also observed in Figure A.1. Transport cospectra also reflects the findings in Figure 4.2, with predominantly onshore directed transport for the infragravity wave band and wind wave band, where it is shown as a broad bulge peaking around 0.22 Hz.

For category 3 no clear, distinct peaks are visible for either the concentration or velocity spectra at this selected high tide moment, except for infragravity wave band velocity at 0.017

Hz. The largest transport is found in this infragravity wave band, with two very large peaks at 0.01 and 0.035 Hz, which are significantly larger than the peaks in the wind wave band, which are found between 0.07 and 0.13 Hz. The transport shown is almost exclusively onshore directed.
Lastly, the velocity and concentration spectra for category 4 are quite similar to those of category 3 in that they show no distinct peaks. Most of the transport is shown to take place between the frequencies of 0.05 and 0.2 Hz for incident waves, which is predominantly onshore directed. The overall oscillatory transport is, however, shown to be quite small in the cospectra, which was also noted for the category in Figure A.1.

4.1.2 Tidal variations

In Figure 4.1 (of previous section) cyclic variations were noticeable in the various time series of hydrodynamical conditions. These cyclic variations are associated with the changing water levels during the tides. In this section the differences in effect of the changing tidal water levels on the hydrodynamical conditions between the four categories will be further analysed. Additionally, possible resulting variations in the (relative importance of the) transport components will be discussed.

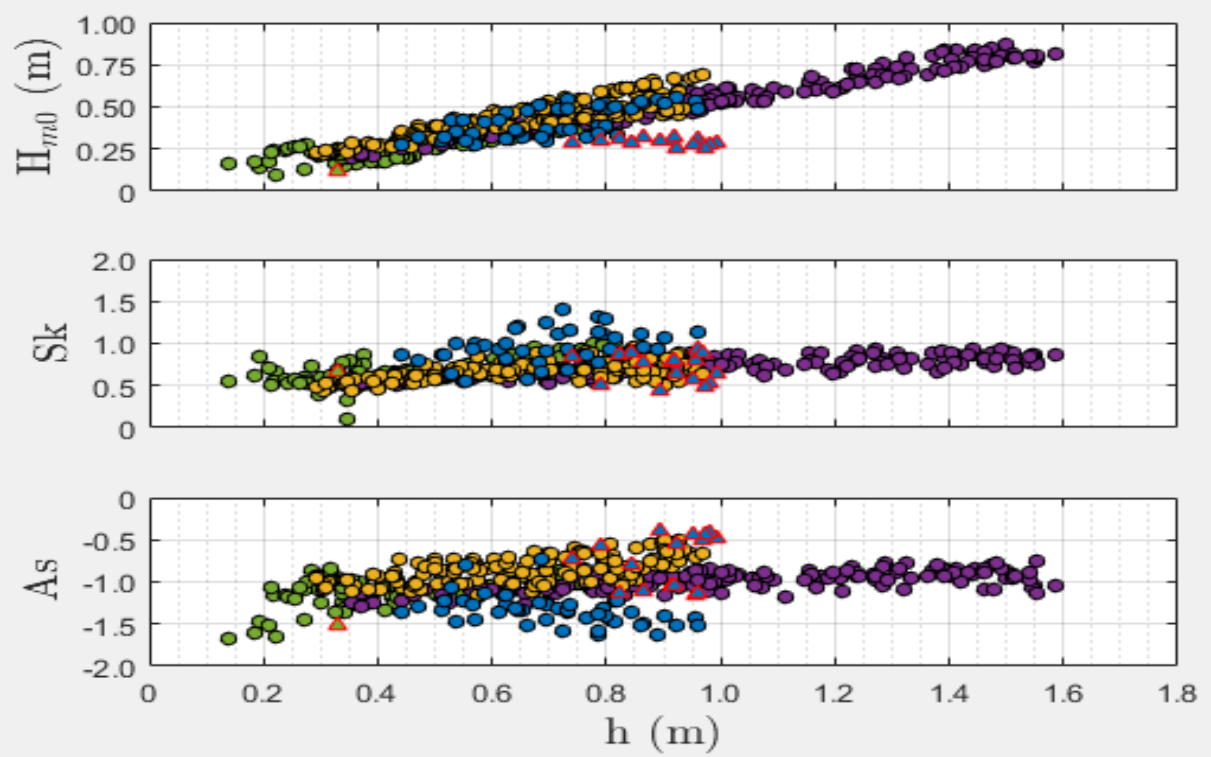

Figure 4.4: Significant wave height (H_{m0}), wave skewness (Sk) and wave asymmetry (As) plotted against water depth, with the categories colour coded (category 1 in blue, category 2 in yellow, category 3 in purple and category 4 in green). Data is gathered by the CRD frames. Results for non-breaking waves ($H_{m0}/h < 0.40$) are displayed with triangular markers with a red edge colour.

Figure 4.4 shows that the local wave height is proportional to the local water depth, and that this linear relation is more or less the same, ranging from 0.41 for category 4 to 0.55 H_{m0}/h for category 2, regardless of category. The single exception is a section of the data from the first category which consisted of non-breaking waves (H_s/h < 0,40), which are found to be unrelated to water depth. Wave skewness follows an upward linear trend (ranging from 0.25 for category 4 to 0.55 Sk/h for category 2, though admittedly with quite a bit more scatter in the data is present than can be seen for wave height) for all categories except of the first, where there is an decrease in skewness with increasing water depth for non-breaking waves within this category; -0.43 Sk/h.
Adversely, wave asymmetry shows an upward trend (ranging from 0.22 for category 3 to 0.55 As/h for category 4) for all categories except for breaking waves from category 1, which displays a downward trend with increasing water depth; -0.63 As/h.

These results show that there is a clear distinction between the trends of breaking and non-breaking waves of category 1; an opposite trend, either upward or downward, distinguish the two datasets. Interestingly, this distinction is not necessarily true when these datasets are compared to the (breaking wave) datasets of the other categories; for wave

a)

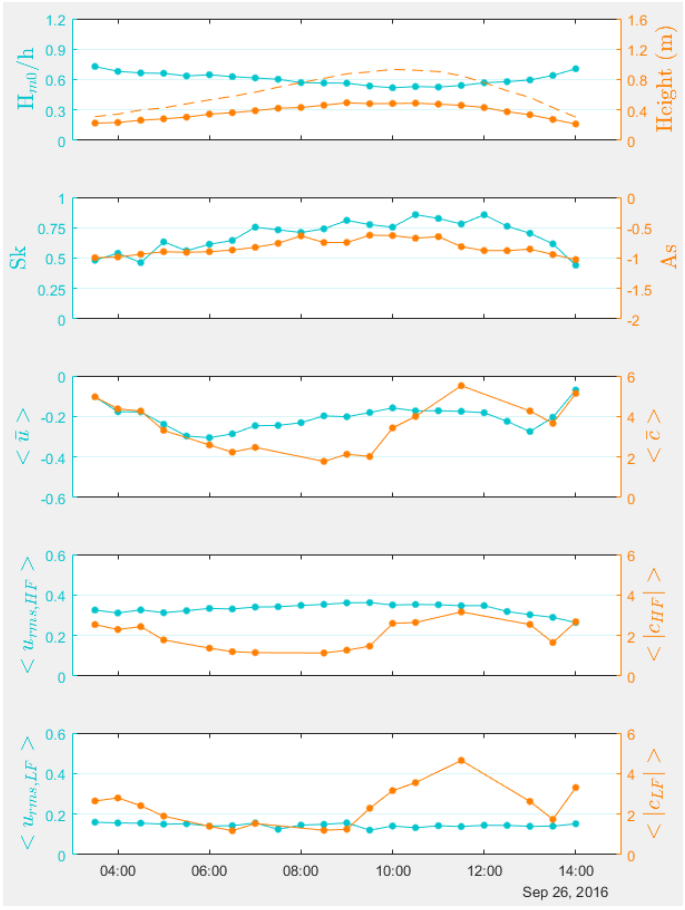

b)

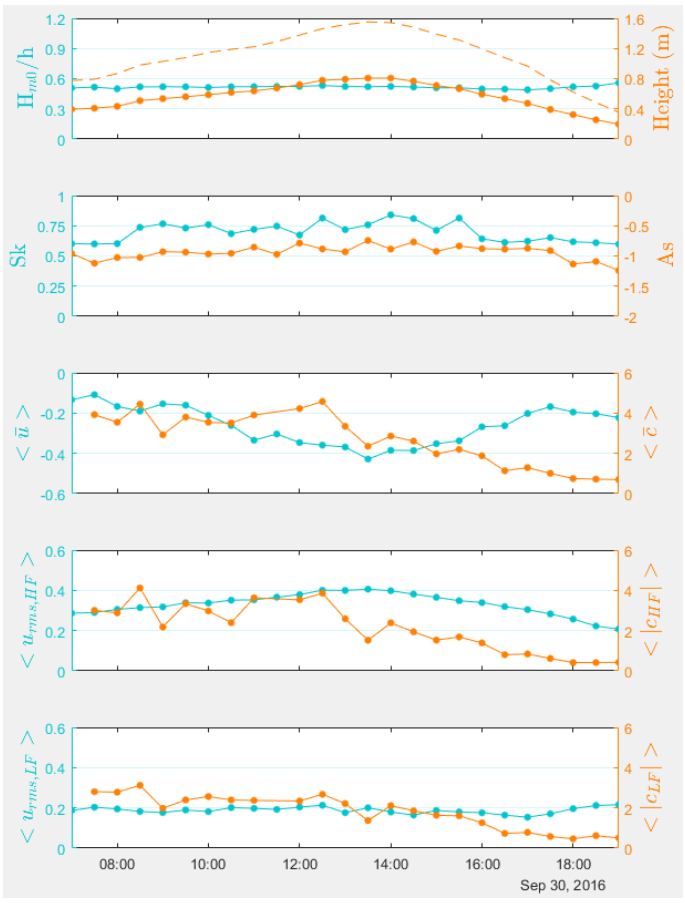

Figures 4.5: Temporal change of various hydrodynamical parameters during a single tide in category 2 (a) and category 3 (b). In the first plot wave height is displayed with a solid orange line, water depth with a dashed orange line, and relative wave height is shown in solid blue. The second plot shows skewness in blue and asymmetry in orange. Velocities are in [m/s], with u_{rms} representing root-mean-square orbital velocities. Concentrations are in [kg/m^3].

asymmetry the data for non-breaking waves follows the same trend as the breaking waves of the other categories. It is uncertain what causes this. Possibly the difference in predominantly plunging breakers for breaking waves in category 1 and a predominance of spilling breakers for most of the rest of the field campaign may be the cause.

By analysing the changing conditions and corresponding transport components for a single tidal cycle (12.5 h, from peak to peak of low tides) for each of the categories, an attempt is made to find the importance of water depth and relative wave height on the magnitude and direction of the net transport and the transport components and their relative importance. The results of this analysis are displayed in Figure 4.5 for the hydrodynamics and Figure 4.6 for transport components of category 2 and 3, and similarly in Figure A.4 and A.5 the hydrodynamics and transport components of category 1 and 4.

During the tidal cycle of category 1 the wave height remained consistent (~0.3 m), an attribute that is not found in other categories but is not characteristic for the entire category (see Figure 4.1). These wave are found to only break at the start and end of the cycle as the relative wave height can be seen to drop below the 0.4 mark (with a minimum of 0.3 at peak tide) for a considerable amount of time (around 5 hours). Wave asymmetry can be seen to decrease in value with increasing water depth (from -1.2 to -0.4), while skewness does not show a clear pattern related to water depth . Both oscillatory currents are found to increase with decreasing water depth while the steady current becomes stronger. All three suspended sand concentration components show the same trend; increase with decreasing water depth.

a)

b)

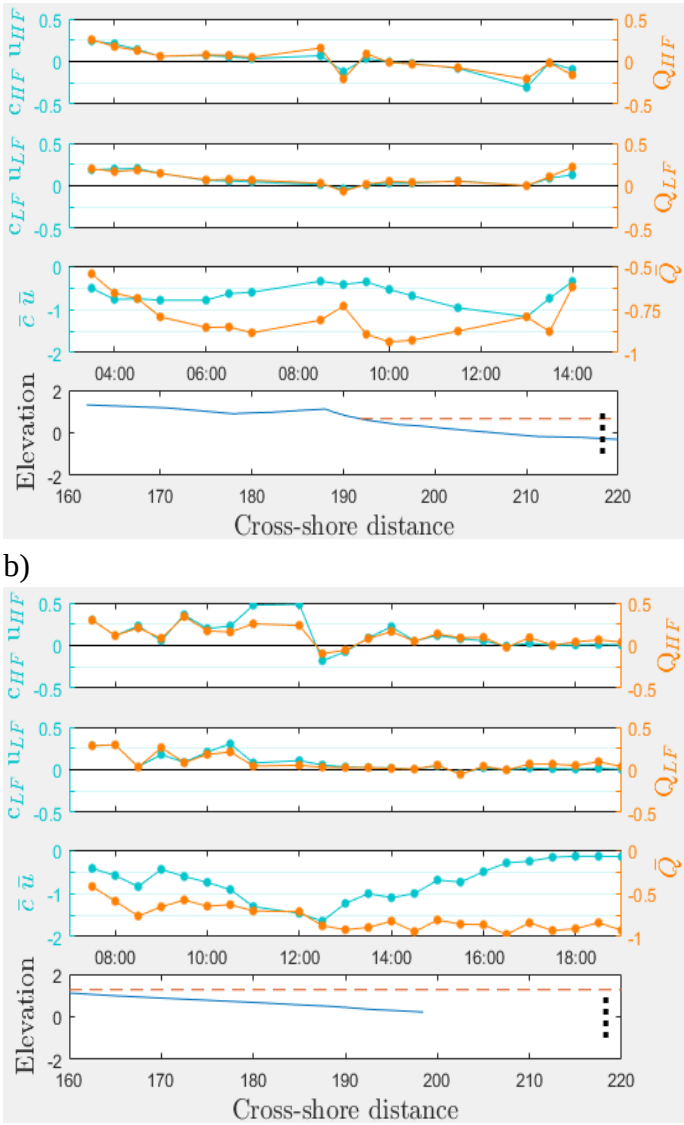

Figures 4.6: Temporal change of the magnitude, direction and relative importance of the transport components during a single tide in category 2 (a) and category 3 (b). First plot shows the HF transport component, second the LF transport component and third transport due to steady currents, all with the transport flux in blue and the fraction with respect to the net flux in orange. The last plot shows the corresponding bed profile in blue with the maximum high water level in red. Black dots indicate the cross-shore position of the CRD frame, where the data displayed here is taken from. Transport rates are in [kg/m^{2}s].

Categories 2, 3 and 4 all show the same trends regarding wave asymmetry and wave skewness. Although relative wave height is found to increase with decreasing water depth for categories 2 and 4 and while categories 3 displays a mostly consistent relative wave height throughout the tide, both asymmetry and skewness decrease for all three categories.
Velocity and concentration components do not, however, show a consistent trend between the categories. For category 2 the steady current has minimum velocities at the beginning and end of the cycle as well as at peak tide (in total ranging from 0.07 to 0.30 m/s, offshore), while HF and LF are found to be mostly consistent throughout the tide (at 0.30-0.35 and 0.12-0.15 m/s onshore, respectively). All three concentration components follow the same trend which seems to be a decrease with increasing water depth, though for all three there is also an inexplicable 4 hour bump in increased concentrations present near peak tide.
Category 3, on the other hand, shows increased velocities with increasing water depth for both steady and HF components while the LF component is once more found to be unchanged throughout the tide. The concentration components of this cycle all seem to be unrelated to water depth, with a downward trend over time. Lastly, all three concentration components for the tidal cycle of category 4 show a mostly increasing trend with increasing water depth. However, only the HF velocity component seems to be related to water depth, with higher values for increasing water depth.

In the results of category 1 the HF transport component seems to follow an erratic pattern that resembles the one of wave skewness. Its magnitude is mostly unrelated to water depth. Its direction is predominantly offshore, with only reversals to onshore directed transport at the beginning and end of the cycle (in the form of a single data point on each end). Its importance, however, does seem to be somewhat related to water depth; highest importance near peak tide (with a value of 0.6) and mostly decreased importance with decreasing depth.

The magnitude of the LF transport component is quite low near peak tide for most of the tidal cycle, but increases considerably towards the start and end (by around a factor of 10). This temporal variance in magnitude is also reflect in the relative importance of the LF component, with significantly higher LF importance at the start and end of the tidal cycle (maximum of 0.14, compared to < 0.05 near peak tide).
The steady component also has maximum transport rates at the beginning and end of the tidal cycle and its influence similarly seems to be mostly related to water depth, with a dominating importance of > 0.75 for most of the tidal cycle but decreases significantly in influence (with a minimum of 0.39 near peak tide) with increasing water depth.
The transport due to steady currents and LF oscillations for this tidal cycle in category 1 are the predominant components during low water levels, but their importance is significantly reduced with increasing water depth with the HF component becoming more important. Interestingly, this increase in importance of the HF component is found to be mostly due to decreased magnitude of both the LF and steady transport components rather than increase HF transport.
In terms of the magnitude of the transport components the first two categories show a different pattern than the last two. For the first two categories the transport flux due to steady currents is smallest at peak tide. For category 1 this is solely due to a decreased suspended

sand concentrations at peak tide as the velocity component was found to be unchanged during the tidal cycle. For category 2 the pattern is much more complicated, with the change in velocity over time being seemingly unrelated to either the change in relative water level or wave shape. Adversely, for category 3 and 4 the transport flux due to steady currents is largest at moment of high water, with high values for sand concentration and cross-shore velocity around high water.

From these figures it seems that the relative importance of the steady component increases with increasing water depth, with the HF and/or LF components generally being smallest at maximum high water for the last three categories. For category 1 the significance of the steady component is, on the contrary, smallest at high tide, explained through the reduced significant wave breaking resulting in less undertow. Additionally, the undertow is partially replaced by rip currents as waves manage to only reach over the intertidal bar near peak tide. The results additionally indicate that temporal changes in the velocity components do not necessarily align with changes in sediment concentrations. Moreover, wave shape (particularly wave skewness) seems to be a decent indicator for the magnitude of the transport components.

As these results are taken from a single tidal cycle for each of the four categories, and the number of data points for particularly the transport components is rather limited, it may not be representative for all tidal cycles for the respective categories. Therefore the conclusions drawn do not have a high certainty. To increase certainty and to further examine the effect of relative wave height and/or wave breaking on the magnitude and direction of the transport components, all the measured transport data has been plotted against local relative wave height (see Figure 4.7).

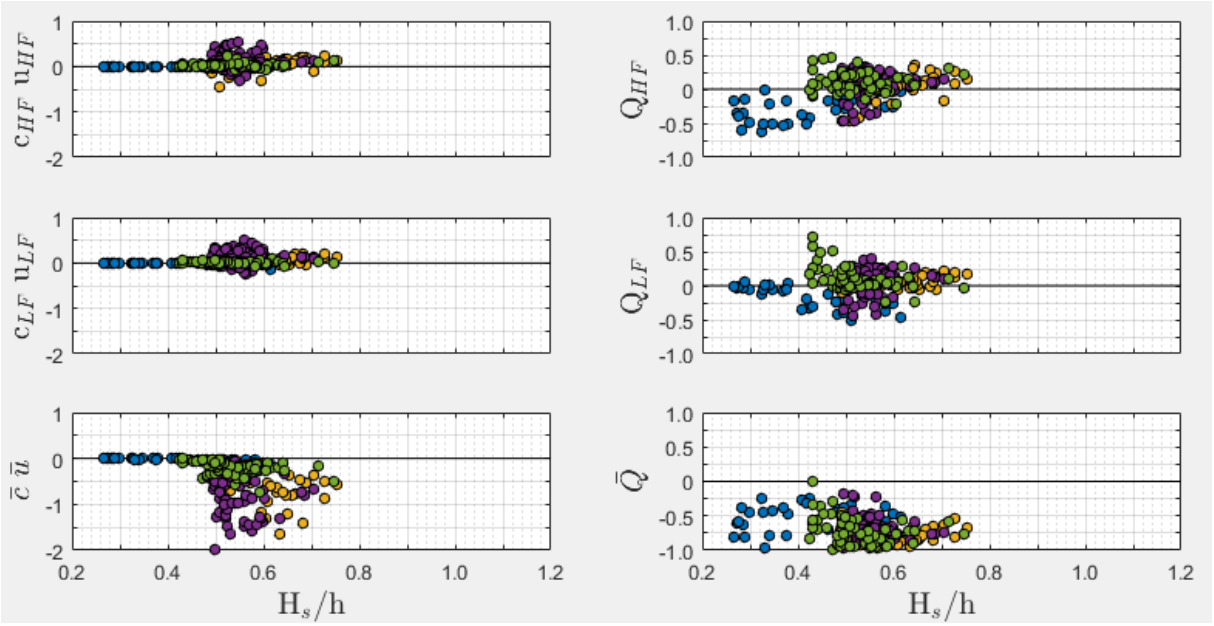

Figure 4.7: Rates (left hand column) and fractions (right hand column) the transport components as a function of local relative wave height at the CRD. Colours represent results from the four categories. Transport rates are in [kg/m^{2}s].

The difference between results of breaking and non-breaking waves is clearly visible in the plot of the normalized transport index (see Figure A.6). Transport rates due to HF oscillations and steady currents are here shown to be exclusively offshore directed under non-breaking waves while the LF component, which is occasionally onshore directed, is nonetheless considerable smaller in magnitude than these other components. The resulting normalized transport index for this category thus shows almost exclusively (near) total offshore transport rates, which forms a clear contrast with the wide range of results for breaking waves from other categories.
Other categories display a far greater dependency on relative wave height. Particularly the results from CRD and miniframe 15 show a tendency for net transport to be onshore directed for lower ratios while being offshore directed for higher ones. Interestingly, this seems to be only true for the data gathered during category 3 and 4, which had highly different wave conditions. It is imagined that the nearshore morphology of a straight, gently sloping shoreface, which is a conformity of the two categories, is the cause of this pattern. Undertow driven steady transport component, which dominates the net cross-shore transport for higher ratios, becomes subordinate to either the HF or LF component at lower ratios; a decrease from a near or complete dominance to a mere 25% while the HF or LF component rises up to a (close to) 50% share.
Results from category 2 show a complete oposite relation in this respect; for increased relative wave heights net transport rates are shown to become predominantly onshore directed. This trend is, unlike the one found for category 3 and 4, not predominantly determined by the dissapeared dominace of the steady component. Instead the combined onshore effect of the two oscillatory components is needed to (partly) negate the offshore directed steady component and decrease the amount of offshore net transport rates, as is shown in the results for CRD, where the onshore LF contributes up to 20% and HF for roughly 30% to net transport. The direction of the subordinate LF component, hovering at around 0-20% for most of the data of category 2, is subsequently the critical factor in determining the direction of the net transport.

The results of Figure A.7 show that when the normalized transport index (Q_d, see Eq. 6) is plotted against the non-dimensional parameter (D, see Eq. 7) for all categories the net offshore directed transport flux can be seen to have a linear relation for a semi logarithmic scale, decreasing in magnitude with increasing value for D, until the transport becomes onshore directed where afterwards it will increases with increasing value for D. The one major exception are the results for category 1 for the CRD which, due to the absence of significant wave breaking, deviate greatly from this trend and is shown to be completely independent of the non-dimensional parameter.
Between $D \sim$ 2-9 net transport tends to switch from predominantly offshore directed to onshore directed for all other categories and for all frames. The general value at which this reversal takes place seems to be partly determined by the energy of the waves, with the results from storm conditions near the lower end and results from swell conditions near the higher end of this range. This is explained through the results of the transport components (Figure 4.8) which shows a tendency of data from categories of higher energetic wave conditions (category 3 and partially category 2) to be found near the lower values of D (mostly ranging

from 1 to 4), and data from lower energetic wave conditions near higher values of D (predominantly found between 3 and 12).

Regarding the change of direction and relative importance of the transport components with respect to the value of D (see Figure 4.8) additional observations can be made. The HF transport component is found to generally increase in importance with increasing value of D. The one exception is in the data of category 4, for which a maximum importance of ~ 0.5 near a value of D of around 1.4 and decreases in importance for both lower and higher values of D. Moreover, the direction of the HF transport changes from predominantly onshore to offshore directed for the few data points with the lowest and highest values of D.

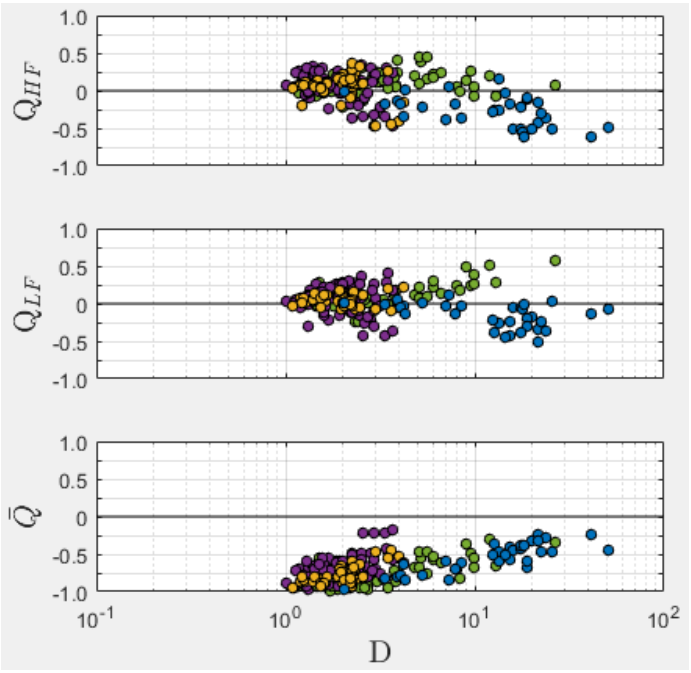

Figure 4.8: Normalized sediment flux index for the net transport flux, and fractions for the three transport components are plotted against the non-dimensional parameter (D). The colours represent the results from the four categories; blue is category 1, yellow category 2, purple category 3, and green category 4. Data taken from the CRD frame.

The direction of the HF transport component only seems to relate to the value of D for category 4, with offshore directed HF transport exclusively found in the data set at the lower and higher values of D. Adversely, for the direction of the LF transport component only the data of category 4 suggests a relation with D, with offshore transport solely found at lower values. Exclusively offshore directed steady components are present in the data displayed.

Through Figure 4.10 the dependency of D on the parameters through which D is calculated (see Eq. 7) is analysed to evaluate what causes the transport reversal for higher values of D. This reveals that the logarithmic nature of D is mostly caused by its relation to the mean currents $\overline{U}$. Additionally, it is found that the value for mean currents generally dominates the resulting value of D as it is only weakly dependent on both $\sqrt{Sk^2 + As^2}$ and U_{rms}. Only for the data of category 1, for which the range of values for $\overline{U}$ is rather limited, is wave shape the dominant component that determines the value of D.

Thus it can be concluded that the magnitude of the mean currents is of greatest importance for the magnitude and direction of net transport for the last three categories, in which the steady transport component dominates over the transport driven by oscillatory currents, both individually or additively.

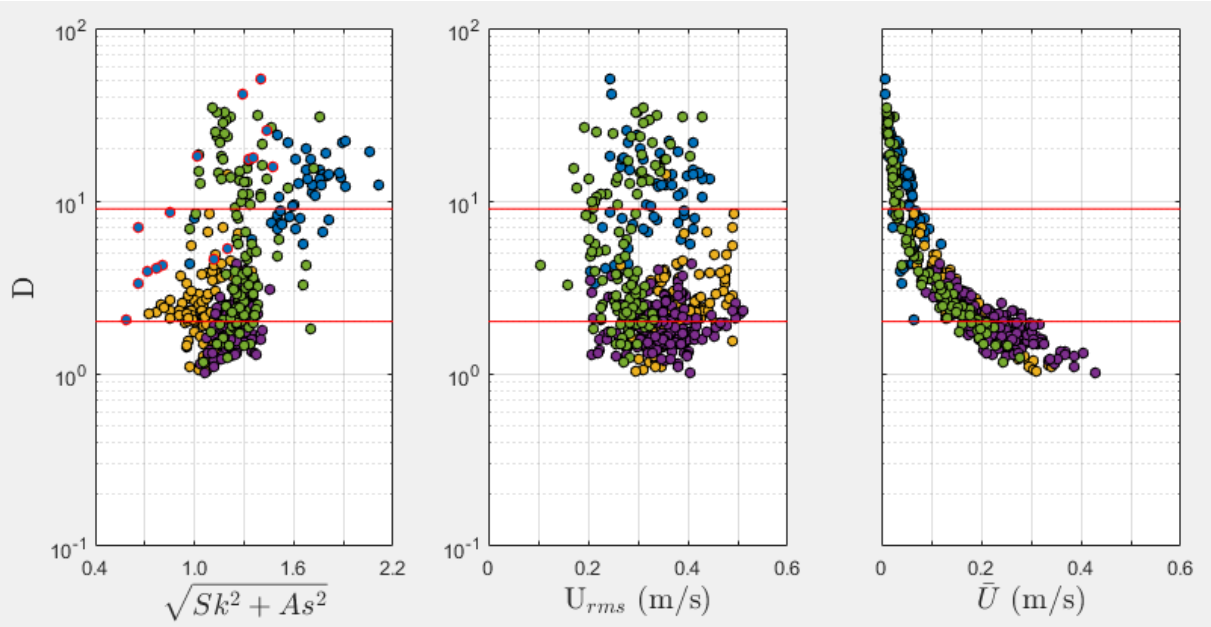

Figure 4.10: Non-dimensional parameter (D) plotted against a parameter for wave shape ($\sqrt{Sk^2 + As^2}$), incident orbital velocity (U_{rms}) and undertow velocity ($\bar{U}$). Data is taken from the CRD frame.

4.2 Spatial change in hydrodynamics and transport

Now that temporal changes in hydrodynamical conditions and the resulting effect on relative transports component importance have been discussed, the focus shifts to their spatial dependence, particularly through cross-shore profiles and the position of the frames with respect to the shoreline.

4.2.1 Cross-shore evolution

In Figures A.8, 4.11, 4.12 and A.9, graphs are shown depicting the cross-shore variability of various hydrodynamical conditions, combined with the direction and magnitude of the transport components and the cross-shore profile, for selected timestamps at different days for each of the categories (1:4, respectively). The relative importance of the transport components are shown in fractions in the form of boxplots, grouped for each frame with the left column of the group representing the results of the first day (blue) and right column of the last day (either purple or green). To make cross-shore variability of the individual transport components more visibly pronounced, the scale of the y-axis is not kept consistent between the transport components, nor between the results of different categories.

For category 1 significant wave height is shown to increase from 0.3 m at the cross-shore position of CRD to a maximum of 0.4 m at miniframe 13, while water depth experiences a steady decrease along the entire frame transect. Resulting relative wave height subsequently experiences a rapid increase from miniframe 13 onwards in shoreward direction, with the waves starting to break at OSSI 3. Wave skewness shows quite an erratic pattern. Wave asymmetry follows a similar trend to wave height, with seemingly increasing asymmetry with increasing wave height to a maximum of 1.1 at miniframe 13.
D is found to decrease somewhat steadily from CRD to miniframe 15 from 18 to 2.

All three transport components, almost consistently offshore directed, can generally be seen to increase in magnitude in landward direction. The boxplots reveal that at CRD the HF component was actually dominant over the steady component with a fraction of 0.6 while the LF component was here negligent. Adversely, the HF component is negligent at the miniframes, while LF component assumes a value of 0.4 and 0.2 for mini 13 and 15, respectively.

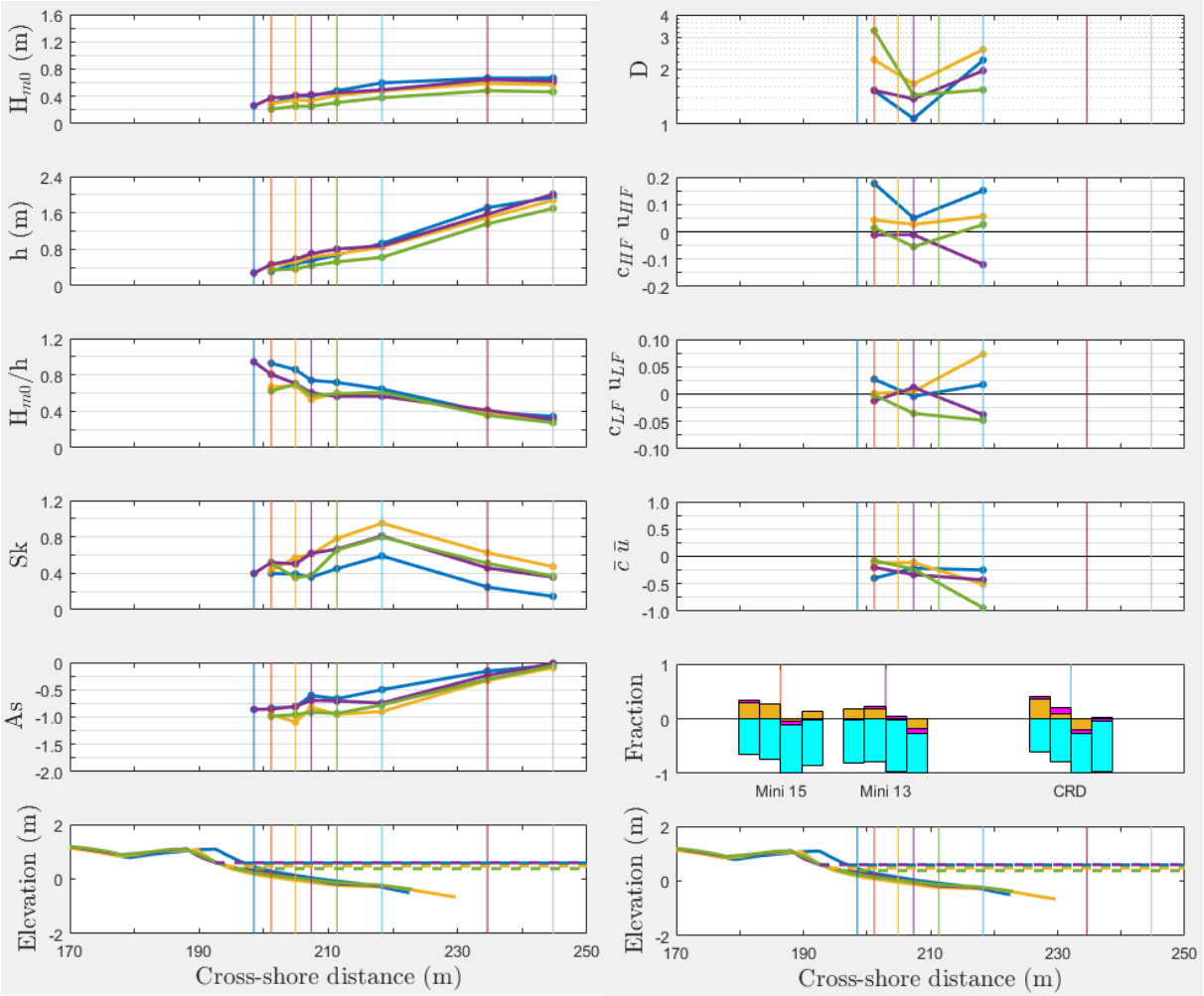

Figures 4.11: Cross-shore evolution of hydrodynamical conditions (left) and sand transport components (right) for category 2. Line colours represent data from different instants during category 2; Blue: 6:30, 23 Sept.; Yellow: 8:30, 25 Sept.; Purple: 9:00, 26 Sept.; Green: 10:00, 27 Sept.. Boxplot colours are orange, magenta and cyan for HF, LF and Steady components, respectively. Transport rates are in [kg/m^{2}s]. Vertical coloured lines indicate the cross-shore positions of the OSSIs and frames (FLTR. OSSI 5, Miniframe 15, OSSI 4, Miniframe 13, OSSI 3, CRD, OSSI 2 and OSSI 1).

Both significant wave height and water depth can be seen to consistently decreases towards the shoreline for the moments selected for category 2. The rate of decrease in water depth, however, is lower for the section of the transect between CRD and miniframe 13.
Relative wave height subsequently increases along the transect in landwards direction but is mostly stable for this section between the two frames. Wave skewness reaches a maximum

value of 0.59-0.95 at CRD and sees significant decrease in both landwards (minimum of ~0.4) and seaward direction (minima of 0.15-0.47). Asymmetry, on the other hand, is found to generally increase (from ~ 0-0.99) with a small local minimum around miniframe 13. The plot of D shows generally significantly lower values at miniframe 13 than at the two other frames. Resulting transport for the three components overall generally decrease (2-11 times smaller). Both onshore and offshore HF and LF transport is found, with the direction of the two components generally in agreement with each other. The fraction boxplots reveal that these oscillatory components are subordinate to the steady transport component, even in their combined effect. While the contribution of the oscillatory currents to net transport is lowest at miniframe 13 with an average of only 20%, these contributions do not change all that much along the transect (~ 22-24% at miniframe 15 and CRD).

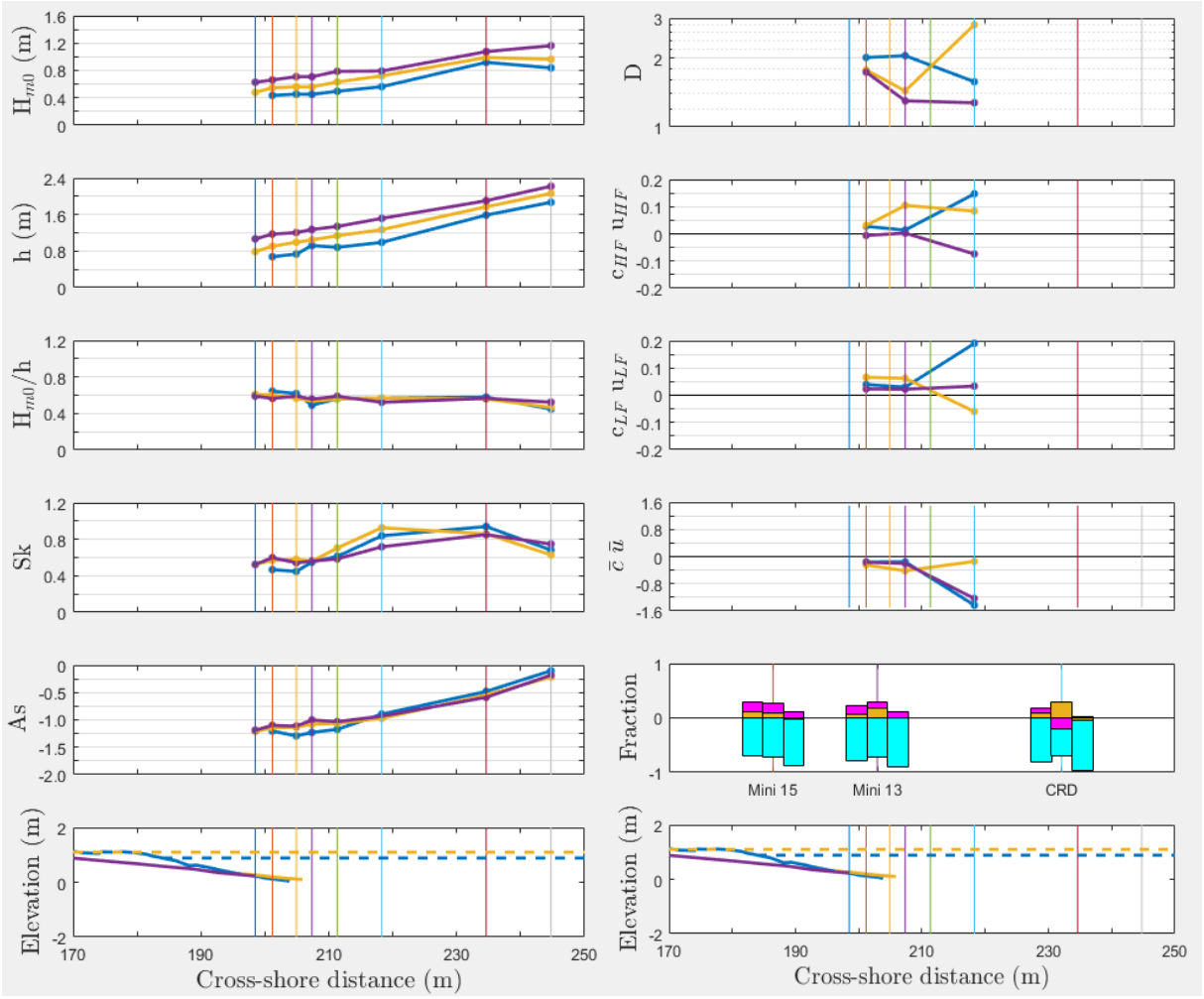

Figure 4.12: Cross-shore evolution of hydrodynamical conditions (left) and sand transport components (right) for category 3; Blue: 9:00, 28 Sept.; Yellow: 11:00, 29 Sept.; Purple: 13:00, 30 Sept.

Quite similar cross-shore variations of the hydrodynamical conditions are found for category 3 and 4. For both categories significant wave height and water depth are found to generally decrease in landward direction. And while relative wave height for category 3 is mostly stable at a value of ~ 0.6 for almost the entire transect, is the increase for category 4 (from ~ 5 at OSSI 1 to 7 at OSSI 5) still rather small in comparison with the cross-shore variance in relative wave height for category 1 or 2. Moreover, the graphs for wave skewness and asymmetry are almost identical between the two categories, with an increase in asymmetry along the transect while skewness decreases landwards and seawards from maxima at OSSI 2 and CRD. This is probably due to the similarities in the nearshore morphology between the two categories, which is a straight, low sloping shoreface.
D is found to increase in landwards direction for category 4, while for category 3 not a consistent pattern is recognizable between the results of the three moments chosen. In terms of magnitude of transport fluxes, all components generally see a decrease along the transect for category 3, while only the steady component decreases along the transect for category 3; position of the largest oscillatory driven transport changes for each moment. Direction of the oscillatory transport components for the two categories is occasionally found to be offshore directed at CRD but exclusively onshore directed at miniframe 15.
The contribution of the steady component, which is generally the dominant component) is largest at miniframe 13 and smallest at CRD for category 3 while the importance of the HF component increases (~ 40% increase) and the LF component, adversely, decreases in importance along the transect (~ 44% decrease). For category 4, the steady component rather decreases along the transect while the importance of both oscillatory components are on average more than three times larger at miniframe 15 than at CRD.

The cross-shore variance in the importance of the transport component is not always consistent within a category, nor between categories. Both moments with decreased and increased steady component importance with decreased cross-shore distance are found for most categories. For particularly category 4, and to a lesser extend category 2 and 3, some moments are shown at which the importance of oscillatory transport components increases rather with further landward position. In most of these cases this decreased dominance of the steady component is predominantly a result of decreased transport induced by mean currents; for none of the moments shown, with the exception of category 1, the decrease in magnitude of the oscillatory currents is as large as the decrease in the steady transport component. Despite this, none of the cases show a dominance of either one of the oscillatory components, nor them combined, over the steady component, with the exception of dominant high frequency component at CRD for category 1.

4.2.2 Cross-shore dependency

To see whether the observations made in the previous section hold true for the bulk of the data, or whether different observation can be made and conclusions can be drawn on the cross-shore dependency of either the direction or relative importance of the transport components, all available transport data is now plotted against cross-shore position. Cross-shore position, as it is used here in this section, refers to the position of the frame with respect to the shoreline at the moment the data was gathered, which varies in time through relative

water level variations (i.a. due to tidal influences and morphological changes at the shoreline). Here the data from the three frames are presented in the same plot and colours are applied to distinguish between different levels of water level elevations, which allow for further analysis of the data past solely frame distance by including a certain aspect of the hydrodynamical conditions. In this case blue represents results from data that was gathered at moments when the water had a depth greater than 1.2 m, yellow for data between 0.8 and 1.2 m, purple between 0.4 and 0.8 m, and the results shown in green were gathered when the water was shallower than 0.4 m.

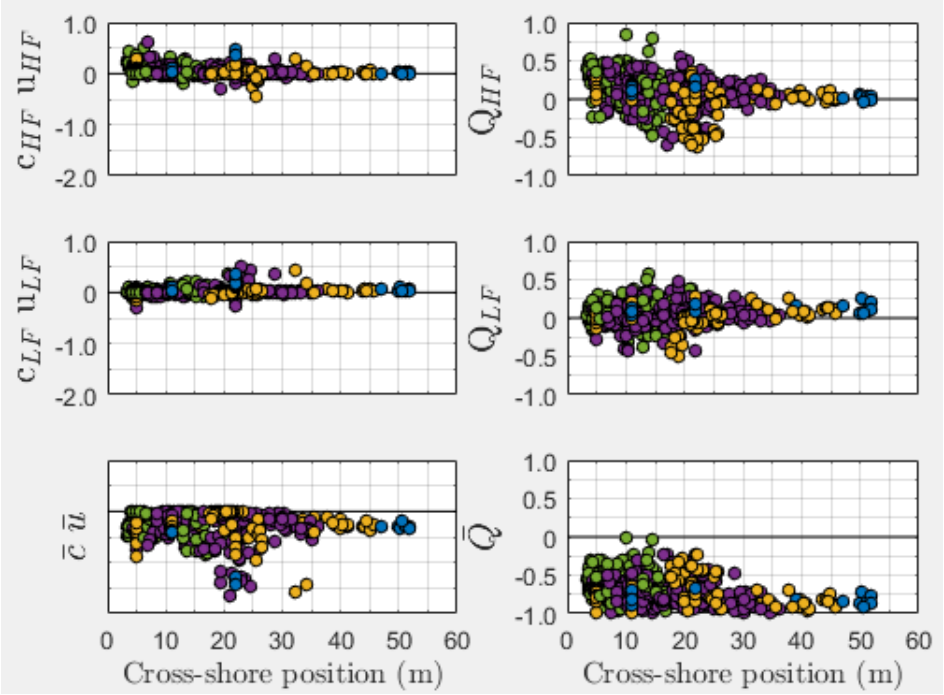

Figure 4.13: Dependency of the transport component fluxes and fractions on the cross-shore distance of the three frames. Colours represent the results from the four water level elevation categories, with blue for h > 1.2 m, yellow for 0.8 > h > 1.2 m, purple for 0.4 > h > 0.8 m, and green for h < 0.4 m.

HF and LF transport components generally see an increase in importance when moving closer to the shore, while the steady component generally decreases (see Figure 4.13). This trend is mostly true for all four of the water level elevation categories. Difference between the four categories, however, is amount of change in importance. Once more the largest importance of both the oscillatory components is found for the category with the lowest water depth (green) and this importance seems to decrease with increasing water depth, which was also observed in section 4.1.2.

The results are bit ambiguous regarding a trend in direction of these oscillatory components; both onshore and offshore directed HF and LF components are found at near-shore positions, while further offshore these components are almost exclusively onshore directed. However, the amount of data for further cross-shore positions is rather limited, despite all available data being shown.

This increased importance of the oscillatory currents for the shallower waters of further shoreward positions may result in the steady transport component becoming subordinate, and depending on the direction of the oscillatory currents (which for either one or both may still be offshore directed), may result in net onshore transport. Figure A.11 illustrates this point, with net onshore transport exclusively found within 30 m distance of the shoreline for the two categories with the most shallow water.

Figure 4.14 compliments these findings to a certain extent, with generally higher values for D found at closer positions to the shoreline than further seawards, exceeding the threshold range of 2-9 (identified through Figure A.7) almost exclusively past the ~ 35 m mark. Interestingly, quite a few data points for the category with a water depth between 0.8 and 1.2 m are found to exceed even a value of 9 for D, between 15 and 25 m offshore. However, no net onshore transport was measured for this category. Figure 4.13 reveals that despite the large importance of the oscillatory transport components in this section of the data, the individual oscillatory components did not align in their direction and thus, through their opposite direction, never managed to cancel out the (occasionally) subordinate steady component. This shows that while the value for the non-dimensional parameter may, to a certain extent, be indicative of the relative importance of the oscillatory and steady transport components, it can not reliable predict the direction of the resulting net transport.

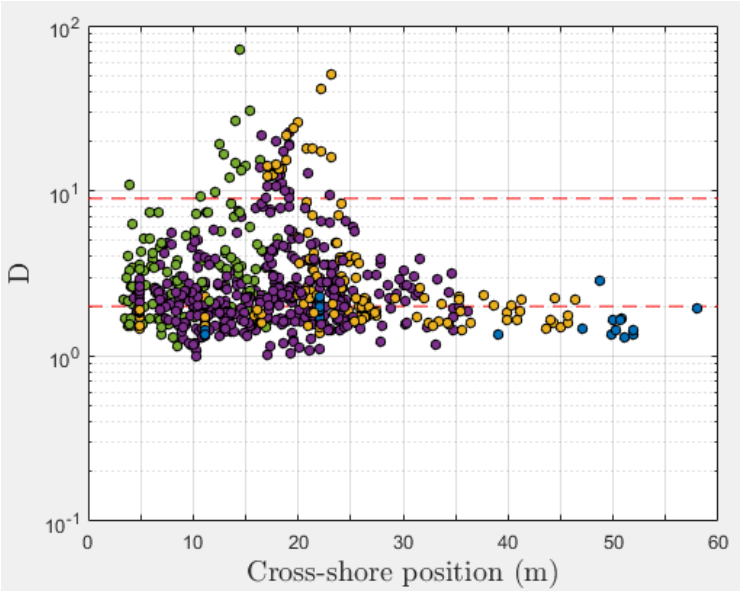

Figure 4.14: The non-dimensional parameter D plotted against cross-shore position. Colours represent the results from the four water level elevation categories.

5 Discussion

5.1 Answering research questions

5.1.1 Research question 1:

The results of the temporal hydrodynamics and transport development (Figures 4.5, 4.6, A.4 and A.5) are in agreement with some of the findings of Aagaard (2002). High water levels were found to be associated with large incident wave heights (with category 1 being the exception due to the absence of sea waves). Aagaard (2002) suggested that this may be due to decreased offshore frictional dissipation. A clear trend in the form of increased mean currents with increased water levels is however not recognized in these results. The results did show that increased water depth generally meant an increase in the relative importance of the steady component, possibly due to the increased wave height with increased water depth. For category 1 the opposite was true, possibly due to the limited wave height which prevented wave breaking. Additionally, undertow was partially replaced by rip currents due to the presence of cell circulation which may only have been active at higher relative water levels (when waves were able to overtop the intertidal sandbar near the shoreline).

Aagaard et al. (2013) plotted their net transport fluxes data, gathered from beaches with various states (dissipative, intermediate and reflective), against local relative wave height and found that the transport tended to be onshore for small ratios, turning offshore as the number became larger only for it to revert back onshore at a certain point. For their Vejers dataset, which was gather just seawards of the crest of a subtidal bar located ~ 125 m from the shoreline, the reversals between onshore and offshore directed transport were found at 0.4 and 0.85, respectively. The trends in the results of Figure A.7 are comparable with the findings of Aagaard et al. (2004, see Figure A.7). The biggest takeaway is that the trend is similar for categories 2, 3 and 4, while the graph presented in Aagaard et al. (2004) included results solely from high energetic storm conditions, on both an intermediate state and a dissipative state beach. This shows that these findings at shallow water, inner surf zone conditions of an intermediate state beach are similar to the findings in deeper waters of the surf zone of dissipative or intermediate state beaches. Moreover, these trends are not exclusive to high energetic, storm wave conditions, but can also be found during low to moderate energetic wave conditions. Only the data for swell conditions, either breaking and non-breaking waves, deviates significantly in its trend, as the HF component was exclusively offshore directed under these conditions.

Net transport for categories 3 and 4 was found to have tendency to be onshore directed for lower relative wave heights while being offshore directed for higher relative wave heights. Results of category 2 show the opposite effect. This was due to both oscillatory transport components turning onshore directed and increasing in importance for higher relative wave heights, where their combined effect was able to offset offshore transport induced by the steady currents.
Through the use of non-dimensional parameter D, which is calculated by wave shape, incident orbital and undertow velocity, some order in the scattering of data is achieved. For higher

values of D net transport has a tendency to be onshore directed as the importance of the steady currents decreases significantly as the importance of both oscillatory currents increases. The results from (nonbreaking waves of) category 1 deviates from this as, despite the high relative importance, the oscillatory transport components were almost exclusively offshore directed. The logarithmic property and value of this D is predominantly determined through the velocity of the undertow, which subsequently makes it an important indicator of the relative importance of the transport components and direction of the net transport for breaking waves.

5.1.2 Research question 2:

The steady transport component is found to generally decrease in importance with decreased distance from the shoreline. For positions further seaward the steady component was exclusively found to be dominant over the oscillatory currents, resulting in offshore directed net transport. Where the oscillatory components are onshore directed at positions closer to the shoreline, net onshore transport may take place. This only occurred when the water was rather shallow (below 0.8 m). The non-dimensional parameter did generally show higher values for the positions closer to the shoreline, exceeding the threshold identified for which net onshore directed transport may take place, compared to further seaward positions. However, these higher values were also found for water depths between 0.8 and 1.2 m, for which no net onshore directed transport was actually measured. This suggests that the non-dimensional parameter was incorrect in its "prediction" of net onshore directed transport for this portion of the data. It can thus be concluded that higher values of non-dimensional parameter is an indication of a larger relative importance of the oscillatory currents, but not the direction of these individual component; generally both onshore directed high frequency and low frequency is needed to overcome the offshore directed transport induced by undertow, which is shown to only occur in relatively shallow water (< 0.8 m), close to the shoreline (< 30 m).

As the field campaign focussed exclusively on the inner surf zone, and no data is available for when frames were positioned on both sides of the sandbar, it is not possible to comment on potential cross-shore variations in the relative importance of the transport components with respect to the position of an intertidal sandbank; namely the presence of a infragravity transport reversal at the crest of the (intertidal) sandbar with an onshore directed LF component on the seaward side and offshore directed transport on the landward side, as was described by Aagaard and Greenwood, 2008.

5.1.3 Research question 3:

The low to moderate energetic wave conditions experienced during the first few weeks (category 1 and 2) and last week (category 4) of the field campaign, during which onshore sandbar migration was measured, were not met with net onshore directed transport fluxes in the shallow surf zone. The predominance of net offshore directed transport recorded throughout the campaign, even for these categories with low to mild energetic wave conditions and subsequently onshore sandbar migration, seemingly goes against the hypothesis and literature that the sandbar migration is predominantly driven by suspended sand transport.

5.2 Comparing with previous research

Initially it was cited that according to the literature under low and moderately energetic wave conditions wave-induced transport onshore transport would to some extend balance out, and possibly even overcome the undertow-induced offshore transport to result in net onshore directed transport. Adversely, for high energetic storm conditions net transport undertow driven transport would dominate over the oscillatory transport component, and therefore result in offshore direct transport.
The boxplot results from Figure 4.2 do not always match up with these expectations. The steady transport component driven by the undertow is almost consistently larger than the sum of the high frequency and low frequency transport components, regardless of the category. For the CRD a total of only 14 instances of net onshore transport over 30 minute sections have been recorded, 25 instances for miniframe 13 and 26 for miniframe 15, some of which were recorded during the storm conditions of category 4 rather than exclusively during low or moderate energetic wave conditions which would be more in line with the expectations.

There are a couple of possible explanations for the lack of onshore transport fluxes in the dataset. Theoretically there is a possibility that the mechanics behind the sandbar migration are similar to antidunes found in fluvial environments. Since the net flow velocity measured during the high tides was offshore directed the results suggest that the sandbar migrated against the water flow, in 'upstream' direction. Problem with this interpretation is that unlike rivers, where sediment can continuously be supplied from sources further upstream, the shore has a boundary in the form of a beach and dunes from where no or rather limited amounts of sand is supplied, assuming that aeolian transport is minimal or non-existent. Additionally, the cross-shore profiles indicate that the sand budget of the beach actually increased over time, refuting the idea that the beach was the source for the sand in the sandbar, disregarding possibilities of net longshore sediment transport gradients on the beach or in the nearshore region.
Instead, it seems more plausible that previous research is correct in their conclusions that bar migration can in fact, at least qualitatively, be explained through sand transport fluxes (e.g. Aagaard et al., 1998), and that the datasets of transport rates used in this research do not reflect the true net transport fluxes experienced in the inner surf zone.
For one, with the instrumentation of this field campaign only suspended sand transport rates were measured. As such potential net onshore sand transport as a result of high rates of onshore bedload transport, possibly due to landwards bed ripple migration, can not be explored. Additionally, the choice was made to only gather data in the lowest part of the water column, between 0.01 and 0.10 m above the bed, since sediment concentration here are generally highest. When the flow is vertically segregated, as is generally the case on beaches with a mostly straight or weakly crescentic sandbar (Short, 1996), direction and magnitude of the mean currents varies throughout the water column. Variance in instrument height above the bottom can therefore influence the resulting transport rates measured.

To analyse how and to what extend net transport and the HF, LF and steady components of velocity change with position of instrument in the water column, these are plotted against relative instrument height (see Figure 5.3). For this section no adjustments have been made to

the interpolated instrument height time series. Therefore, results may show negative instrument heights. As such, not all data points in the results may be reliable, but it is expected that conclusions can still be drawn.

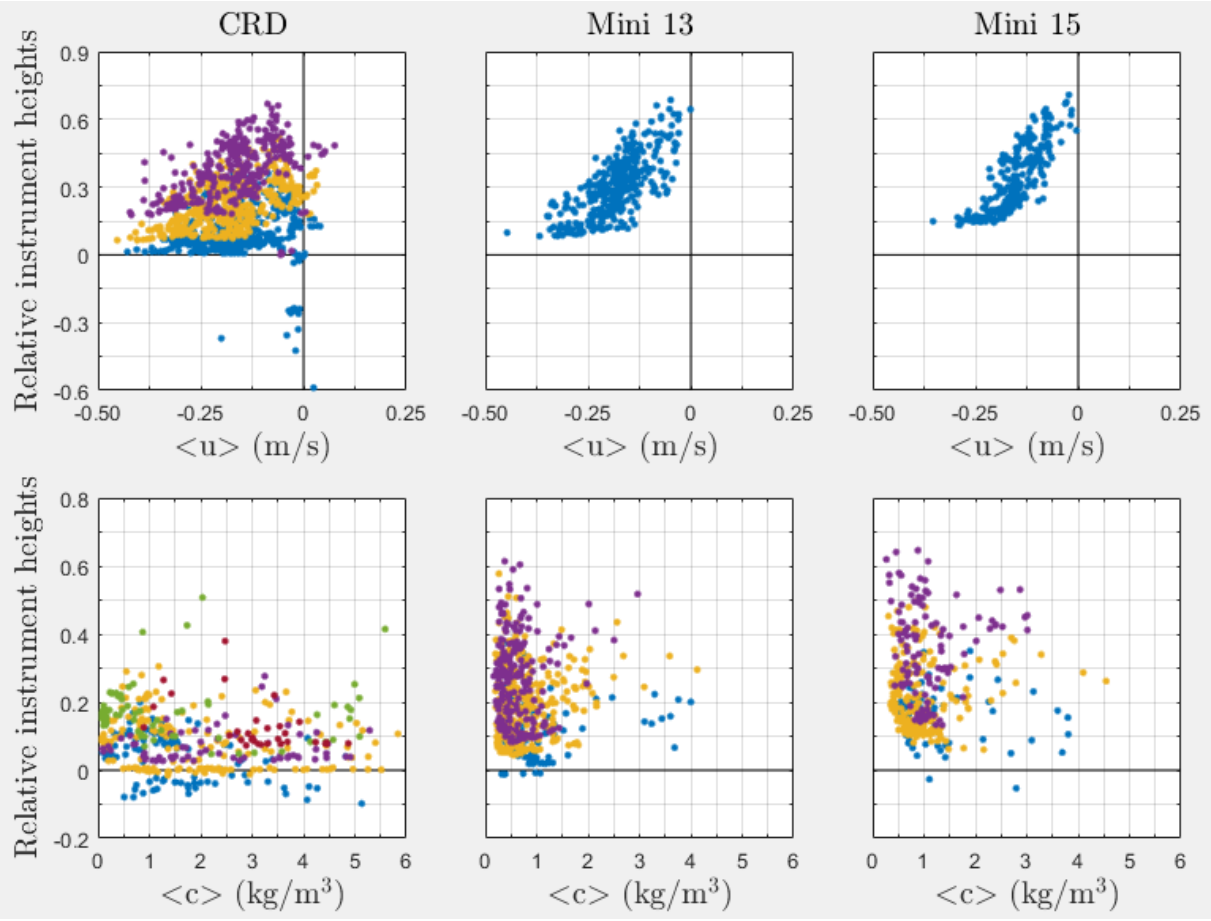

Figure 5.1: Vertical profiles of net velocity and concentration for the three frames. The different colours represent data from different concentration measuring (STM/OBS) instrument numbers, in order of blue, yellow, purple, green and Bordeaux red for the lowest to highest positioned instrument.

The time averaged, steady velocity component is shown to decrease linearly with increasing relative distance from the bed, decreasing from a maximum of 0.48-0.37 m/s undertow close to the bed (0.1 times water depth) to near null velocity in the upper part of the water column (0.6 times water depth). Limited amounts of data of onshore directed currents is reported for CRD, with only a maximum of ~ 0.10 m/s. While quite an chaotic plot is shown for the suspended sand concentration measured by CRD, the results from the two miniframes do suggest a decrease in maximum concentration with increasing height, ranging from 4.0-4.5 in the lower part to 0.7-1.0 kg/m^3 in the upper part of the water column.
Maximum net cross-shore transport profiles (Figure 5.3) also show to be related to the relative position; exclusively offshore directed and relatively large rates are shown for the lower part, while much smaller and occasionally onshore directed transport has been found higher up. This suggests that as the velocity of the undertow and the corresponding steady transport component decreases with increased height, transport due to oscillatory currents may become

of greater importance and may result in net onshore directed transport. The relative importance of the individual transport components on the net transport do seem to depend on the position in the water column.

Further analysis of the vertical position dependency of transport components is done through Figures 5.2. For all three frames the oscillatory transport components are shown to turn predominantly landwards from the lower to higher part of the water column. For particularly the two miniframes increased position is met with increased relative importance (see Figure A.11) of the oscillatory components, mostly due to decreased undertow driven mean rates, resulting in an increased amount of onshore transport. Consequently, net transport higher up in the water column is generally found to be onshore directed (see Figure A.12).

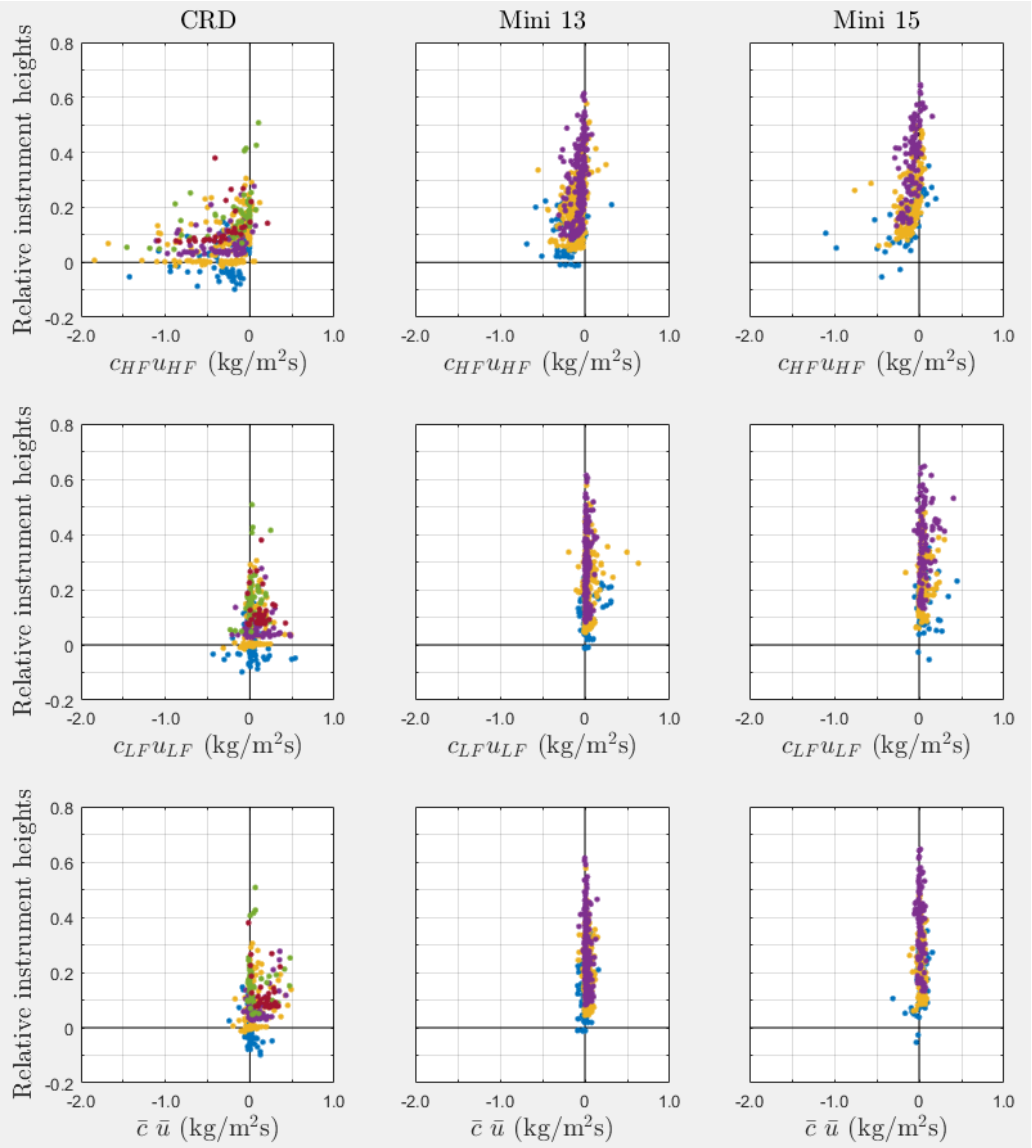

Figure 5.2: Vertical profiles of the transport component rates for all frames. Colours represent data from different STMs/OBSs.

While the lowest part of the water column (< 5 cm above the bottom) was not found to be dominated by (onshore directed) incident wave transport, unlike what was found by Conley and Beach (2003, see Figure 5.3), the decrease in net offshore directed transport rates as a result of the relative increase in importance of the wave transport further away from the bottom (> 5 cm in Figure 5.3) is recognized in Figures A.11 and A.12.

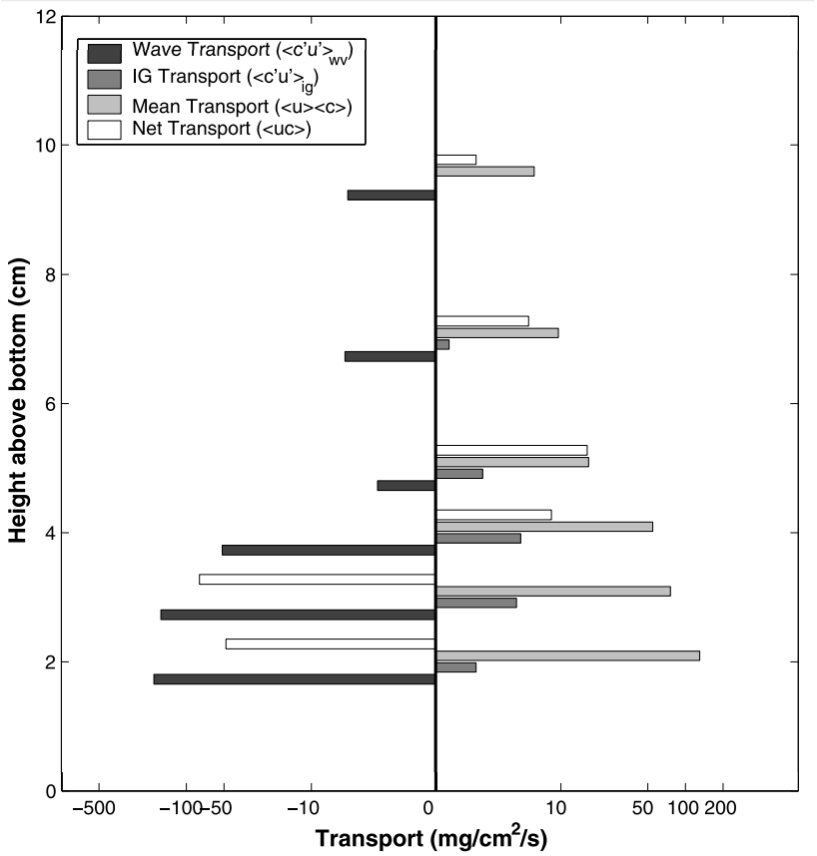

Figure 5.3: Flag plot indicating the vertical distribution of various spectral components of transport for one run at Cluster G. Values represent averages of all valid subruns at each elevation. This figure shows the change in direction of net transport with elevation that can occur because of the increasing importance of wave coherent transport near the bottom. The transport scale is logarithmic and all values with an absolute value less than 1 have been ignored. Offshore transport is positive. (source: Conley and Beach, 2003)

Another possible explanation for the problem at hand may be that the hydrodynamical conditions and corresponding transport rates recorded throughout the field campaign, which were almost exclusively recorded during high tide with the exception of the storm event, are not indicative of those experienced during low tide. When, rather than only using 30 min sections for which at least 90% of the duration raw data was available, all sections are analysed the results seem to indicate that that is indeed the case (see Figures). Do note that the resulting transports calculated for the sections that did not consist of at least 90% data (indicated with red markers in the figure) are less reliable; they may give a distorted view of the real transport during these sections, as explained earlier in the *Data processing* section. This extended dataset has been filtered with the same screening process as the data used for the data analysis.

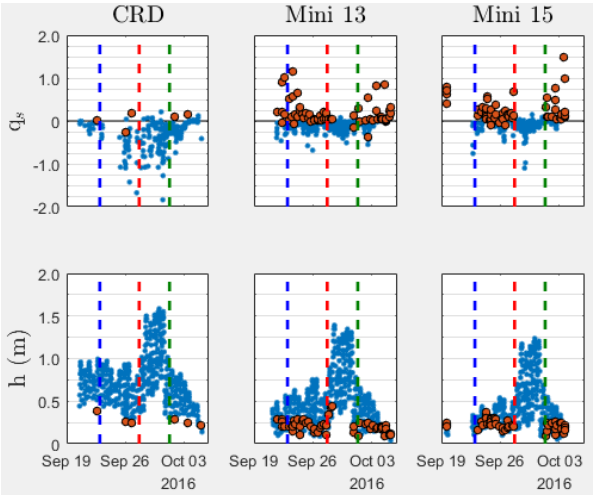

Figure 5.4: Visualization of the predominantly net onshore transport and appurtenant water depths in the extended dataset, gained when all data sections are analyzed, regardless of the percentage of raw data.

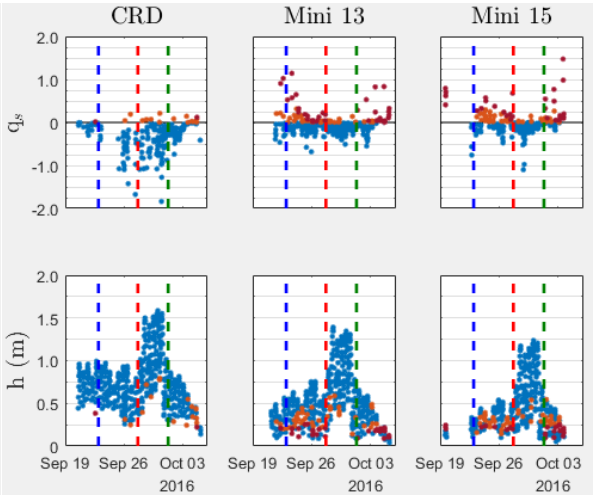

Figure 5.5: Visualization of net onshore transport due to oscillatory currents (orange) and due onshore steady components (Bordeaux) and appurtenant water depths in the extended dataset.

Figure 5.4 shows that the newly included data points gathered from incomplete data sections consist predominantly of net onshore transport while these points were gathered exclusively at moments of low water depths. If these results are indicative of the conditions during low tide, before the frames emerge from the water, it is safe to assume that the onshore transport deemed necessary for the onshore migration of the sandbar took place during low tides. Moreover, in Figure 5.5 net onshore transport solely due to oscillatory currents are distinguished from the data with concurrence of onshore directed oscillatory and steady currents, and the water depths in which these were measured. Onshore directed transport due to steady currents are found exclusively in very shallow water, less than 0.3 m deep.
Far less new data points are included for the CRD frame than the two miniframes. While the fact that the CRD frame was positioned further offshore and thus generally experienced deeper waters might have played a role, it was mostly a difference in instruments used and the corresponding calibration and data preparation process. Since the CRD made use of an ADV for measuring the currents in the water, which measures the water flow through three sensors with a focal length of 0.18 m beneath the instrument itself, it is more susceptible for gathering faulty data during low water levels, influenced by a layer of air between the sensor and the focal point when the sensors are positioned above while the focal point is located beneath the water surface. To prevent the inclusion of this faulty data, which consists of data time series with gaps, it had already been removed before the screening and data analysis. For the miniframes this is not a problem as the EMFs used on the miniframes measure directly at the sensor height and thus only collect data when the instrument is sub-composite.
The newly gained results are highly unreliable and, if that, may only be used as an indication for the direction of the net transport that took place during low tide. Therefore, further analysis in for example linking the magnitude and direction of the transport (components) to the onshore migration (rate of moment) of the sandbar as was intended with research question 3, is not possible.

5.2.1 Longshore variability and cell circulation

It is hypothesized that the onshore net transport fluxes which are presumed to have taken place during low water are in part subject of cell circulation induced by the longshore variability in the intertidal sandbar (Masselink et al., 2008). Only when longshore variability of the intertidal sandbar becomes more pronounced or relative water levels are low may the local undertow be completely replaced horizontal cell circulation in the intertidal zone, resulting in onshore-directed mean currents over the bar crests . This horizontal cell circulation makes use of trough between the slip-face bar and beach as a runnel and outflow channels crossing longshore depressions in the bar crest elevation to divert the water back to the sea. Such outflow channels were observed in the field during the first two and last categories (example in Figure 5.6).

The photograph was taken standing on the left hand side of the frame transect and looking in south/south-westward direction out on part of the research area. The longshore trough, which acts as an overwash and swash fed runnel and is active during high, is clearly outlined by the ripples in the sand.

Figure 5.6: photograph taken on the 4th of October during low water depicting an almost completely drained trough between the beach (left) and intertidal sandbar (right) by the drain in the distance.

Dominant cell circulation and possible corresponding net onshore transport would have only been present during very shallow waters near the bar crest as almost exclusively offshore, undertow driven mean currents have been recorded during higher water levels. Rapid onshore migration rates in the order of 10-20 m per day have been reported under these conditions (Aagaard et al., 2006). The maximum recorded migration rate during this campaign was ~9 m from the 4th to the 5th of October during the fourth category, a couple of days after the storm event. Only a maximum of ~ 5 m per day had been recorded during the first category and the rate reduced as time went on till it became mostly stationary during the second category. The lower migration rates in comparison to those reported by Aagaard et al. (2006) may be explained by the lower relative water levels.

It was found that around the end of category 1 the sandbar had been pushed far enough up the beach face that neap tide water levels experienced throughout category 2 (Figure 3.7) were unable to reach over the crest. While initially the hydrodynamic conditions for this particular category were deemed to favour onshore sandbar migration and thus net onshore transport within the surf zone and this was found to be the case during low tide through what may have been the cell circulation, the sandbar had surpassed the surf zone and was now only subject to continuous wave runup and occasional overwash near the maximum high water levels. Onshore directed steady component and consequently onshore net transport had disappeared

as the cell circulation was replaced with swash-backwash processes. This morphodynamical setting can be said to have partly overridden the nature of low to mild energetic wave conditions to result in local net offshore sand transport, even during low tide. This was expressed in the field through steeping of the seaward slope of this bar. A somewhat similar scenario of morphodynamic feedback with the low hydrodynamic processes was experienced by Aagaard et al. (2004 and 2006); cell circulation which induced an onshore directed steady component during high water were halted and replaced with mean offshore directed transport from undertow. In this example the change was not set into motion by limited water level elevation, but rather the disappearance of the runnel landwards of the bar, which is a necessary component for the cell circulation, as the bar had migrated far enough in landward direction to fill the runnel and form a berm.

5.3 Suggestions for future/further research

The inability of associating sand transport and onshore bar migration is similar to the difficulties experienced by Voulgaris et al. (1998) and Stepanian et al. (2001). Measuring sediment transport rates and monitoring onshore ridge migration in the shoaling wave zone of a ridge-and-runnel system during low-energetic wave conditions, but not being able to gather any or sufficient enough data points of net onshore sediment migration to explain the observed bar migration, they subsequently hypothesized that (bedload) transport due to wave breaking and swash-backwash in shallow water may be vitally important for onshore transport and that the swash processes may possibly be the predominant factor in onshore bar migration. Likewise to this research, the lack of available data from low water made it impossible to confirm their hypothesis. For our research the relative importance of surf-zone processes or swash processes (and subsequent spatial cross-shore variances in the transport components) on the migration of the sandbars has therefore still not been established.

It seems that if one aims to find direct links between onshore sandbar migration and sand transport (components) in the inner surf zone, transport data of particularly the very shallow water and swash conditions needs to be collected. It is recognized that gathering data under these conditions is rather challenging, partly because current available instrumentation has the tendency to cause considerable flow re-direction which negatively affects the quality of the data gathered. Additionally, these conditions tend to produce the largest morphological changes, which may lead to instrument creating scour holes or becoming buried within the bed; problems encountered during this field campaign, despite the daily readjustment of instrument to several centimetres above the bed. Butt and Russell (2000) suggest using fibre-optic backscatter sensors (FOBS/UFOBS) in combination with the ADVs as promising solutions. FOBS were deployed on a second large frame, positioned further in the surf zone during the same campaign (see Brinkkemper et al., 2017), but not on the three frames dealt with in this report. Aagaard et al. (2006) deployed several ADVs in combination with UFOBS in the surf zone and successfully recorded sediment transport rates near an intertidal bar crest in very shallow water, measuring predominantly onshore directed net transport rates for < 0.3 m water depths, which conforms with the extended results from Figure 5.4.

6. Conclusions

Results from a 23 day field campaign carried out in the shallow, inner-surf zone suggests that both hydrodynamical and morphological aspects are of importance for the magnitude and direction of net transport, which is determined by the relative importance of the three transport components: high frequency, low frequency and steady current driven transport.

During the first week the occurrence of long period swell waves in combination with a moderately steep shoreface meant that the waves broke rather close to the shoreline. This shoreline was then represented by the crest and seaward slope of the sandbar positioned high up the shoreface. Increased water depth resulted in decreased importance of the steady component at the same cross-shore position. Additionally, for the same offshore wave conditions a decrease in steady component importance was recorded when moving towards the shoreline. The remainder of the campaign, which consisted of extreme shallow water, mild energetic wave conditions on a steep shoreface, a storm event with considerable storm surge and low to mild energetic wave conditions on a low sloping shoreline, all recorded increased steady component importance with further sea ward position. Here, increased water depth did generally result in increased wave heights.

Net onshore directed transport was almost exclusively recorded in shallow (< 0.8 m), nearshore (< 30 m) water. Under these conditions the steady transport component was still generally dominant over the high frequency and low frequency components, but a combined onshore directed effect of the two oscillatory currents made net onshore directed transport possible. An non-dimensional parameter, calculated from variables regarding wave shape, incident orbital velocity and speed of the undertow, was a reasonable indication of the relative importance of the oscillatory components but not their direction. Subsequently, reliable prediction of net onshore directed transport is not possible. Neither for breaking nor non-breaking waves.

Through the absence of sufficient net onshore directed sand transport recorded during mid to high tide, despite observed and measured onshore sandbar migration throughout different low to mild energetic periods within the field campaign, the results of this research suggest that the bulk of net onshore transport takes place during the rather extreme shallow water and swash conditions. The total amount of onshore suspended sand transport rates under such conditions should, in combination with bedload transport (possibly through onshore ripple migration) be enough to combat the almost exclusively net offshore suspended transport measured in the field to result in the tide-averaged net onshore transport thought to be necessary for the onshore sandbar migration.

If this field experiment were to be repeated it is advised to make use of an experimental setup and instrumentation suitable for measuring specifically during low water conditions; sand transport under these conditions is anticipated to be of predominant importance for onshore bar migration.

References:

Aagaard, T., 2002. Modulation of Surf Zone Processes on a Barred Beach Due to Changing Water Levels; Skallingen, Denmark. Journal of Coastal Research 18.1, 25-38

Aagaard, T., 2011. Sediment transfer from beach to shoreface: The sediment budget of an accreting beach on the Danish North Sea coast. Geomorphology 135, 143-157

Aagaard, T., Black, K.P., Greenwood, B., 2002. Cross-shore suspended sediment transport in the surf zone: a field-based paramization. Marine Geology 185, 283-302

Aagaard, T., Davidson-Arnott, R., Greenwood, B., Nielsen, J., 2004. Sediment supply from shoreface to dunes: linking sediment transport measurements and long-term morphological evolution. Geomorphology 60, 205-224

Aagaard, T., Greenwood, B., 2008. Infragravity wave contribution to surf zone sediment transport – The role of advection. Marine Geology 251, 1-14

Aagaard, T., Greenwood, B., Hughes, M., 2013. Sediment transport on dissipative, intermediate and reflective beaches. Earth-Science Reviews 124, 32-50

Aagaard, T., Hughes, M., Møller-Sørensen, R., Andersen, S., 2006. Hydrodynamics and sediment fluxes across an onshore migrating intertidal bar. Journal of Costal Reseach 22 (2), 247-259

Aagaard, T., Hughes, M.G., 2010. Breaker turbulence and sediment suspension in the surf zone. Marine Geology 271, 250-259

Aagaard, T., Kroon, A., Greenwood, B., Hughes, M.G., 2010. Observations of offshore bar decay: Sediment budgets and the role of lower shoreface processes. Continental Shelf Research 30, 1497-1510

Aagaard, T., Nielsen, J., Greenwood, B., 1998. Suspended sediment transport and nearshore bar formation on a shallow intermediate-state beach. Marine Geology 148, 203-225

Airy, G.B., 1845. Tides and waves. Encyclopaedia Metropolitana, Scientific Department, 241-396

Brinkkemper, J., Christensen, D., Price, T, Naus, I., Hansen, A., van Bergeijk, V., van de Wetering, J., Ruessink, G., Ernstsen, V.B., Aagaard, T., 2017. Surf zone morphodynamics during low-moderate energetic conditions; the TASTI field experiment. Coastal Dynamics, No. 127

Butt, T., Russell, P., 2000. Hydrodynamics and cross-shore sediment transport in the swash-zone of natural beaches: a review. J. Coast. Res. 16 (2), 255– 268

Conley, D.C., Beach, R.A., 2003. Cross-shore sediment transport partitioning in the nearshore during a storm event. Journal of Geophysical Research 108 (C3), 3065.

Davidson-Arnott, R., 2010. Introduction to coastal processes and geomorphology. Book.

Hoefel, F., Elgar, S., 2003. Wave-induced sediment transport and sandbar migration. Science, Vol. 299, 1885-1887

Janssen, T.T., Battjes, J.A., van Dongeren, A.R., 2003. Long waves induced by short-wave groups over a sloping bottom. Journal of Geophysical research, Vol. 108, No. C8, 1-14

Jensen, S.G., Aagaard, T., Baldock, T.E., Kroon, A., Hughes, M., 2009. Berm formation and dynamics on a gently sloping beach; the effect of water level and swash overtopping. Earth surface processes and landforms 34, 1533-1546

Komar, P.D., 1998. Beach Processes and Sedimentation, second edition. Prentice Hall, New Jersey. Book.

Komar, P.D., Miller, M.C., 1973. The threshold of sediment movement under oscillatory water waves. Journal of Sedimentary Petrology, Vol. 43, No. 4, 1101-1110

Kularatne, S., Pattiaratchi, C., 2014. The role of infragravity waves in near-bed cross-shore sediment flux in the breaker zone. Journal of Marine Science and Engineering, 2, 568-592

List, J.H., 1992. A model for the generation of two-dimensional surf beat. Journal of Geophysical research, Vol. 97, No. C4, 5623-5635

Masselink, G., 1995. Group bound long waves as a source of infragravity energy in the surf zone. Continental Shelf research, Vol. 15, No. 13, 1522-1547

Masselink, G., Austin, M., Tinker, J., O'Hare, T., Russell, P., 2008. Cross-shore sediment transport and morphological response on a macrotidal beach with intertidal bar morphology, Truc Vert, France. Marine Geology 251, 141-155

Masselink, G., Puleo, J.A., 2006. Swash-zone morphodynamics. Continental shelf research 26, 661-680

Naus, I., 2017. Observations of alongshore variability in intertidal beach development and wave conditions. *MSc thesis. Not yet published.*

Osborne, P.D., Greenwood, B., 1992a. Frequency dependent cross-shore suspended sediment transport. 1. A non-barred shoreface. Marine Geology 106, 1-24

Osborne, P.D., Greenwood, B., 1992b. Frequency dependent cross-shore suspended sediment transport. 2. A barred shoreface. Marine Geology 106, 25-51

Roberts, T.M., Wang, P., Puleo, J.A., 2013. Storm-driven cyclic beach morphodynamics of a mixed sand and gravel beach along the Mid-Atlantic Coast, USA. Marine Geology 346, 403-421

Ruessink, B. G., Michallet, H., Abreu, T., Sancho, F., der A, D. A. V., der Werf, J. J. V., Silva, P. A., 2011. Observations of velocities, sand concentrations, and fluxes under velocity-asymmetric oscillatory flows. Journal of Geophysical Research 116

Ruessink, B.G., Houwman, K.T., Hoekstra, P., 1998. The systematic contribution of transporting mechanisms to the cross-shore sediment transport in water depths of 3 to 9 m. Marine Geology 152, 295-324

Russell, P.E., 1993. Mechanisms for beach erosion during storms. Cont. Shelf Res. 13, 1243–1265

Sénéchal, N., Ardhuin F., 2008. ECORS Truc Vert 2008: a Multi-Institutional International Nearshore Field Experiment. AGU Fall Meeting Abstracts pages B2+

Short, A.D., 1996. The role of wave height, period, slope, tide range and embaymentisation in beach classifications: a review. Revista Chilena de Historia Natural 69, 589-604

Stepanian, A., Vlaswinkel, B., Levoy, F., Larsonneur, C., 2001. Sediment transport on a macrotidal ridge and runnel beach during accretionary conditions. Proceedings Coastal Dynamics '01, Lund, ASCE, pp. 1017-1027

Thornton, E.B., Humiston, R.T., 1996. Bar/trough generation on a natural beach. Journal of Geophysical Research, Vol. 101 (C5), 12.097-12.110

Voulgaris, G., Simmonds, D., Michel, D., Howa, H., Collins, M.B., Huntley, D.A., 1998. Measuring and modelling sediment transport on a macrotidal ridge and runnel beach: an intercomparison. Journal of Coastal Research, 14, 315-330

Wright, L.D., Short, A.D., 1984. Morphodynamic variability of surf zones and beaches: a synthesis. Marine Geology 56, 93-118

Appendix

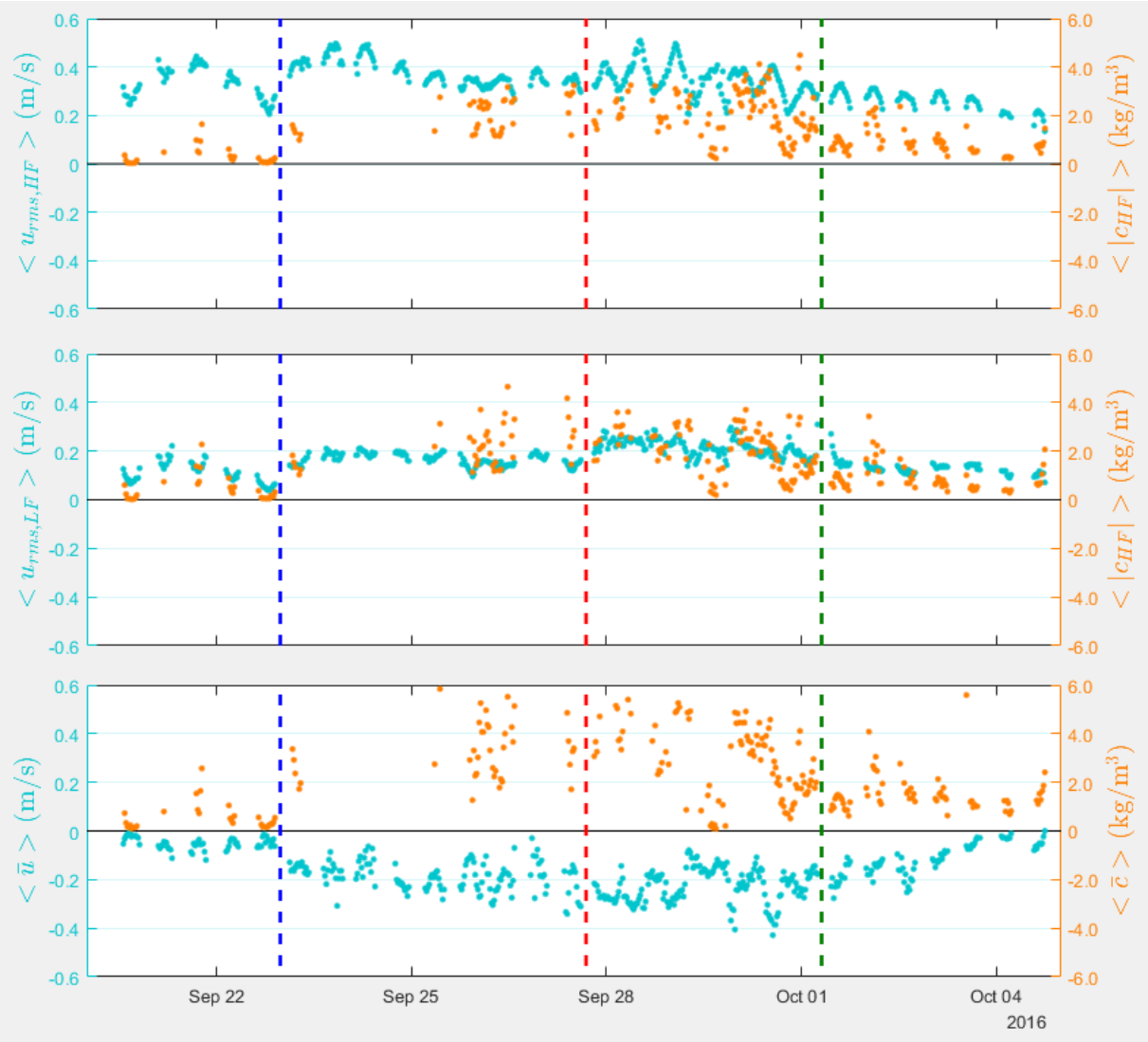

Figure A.1: Time series of the velocity and suspended sand concentration components measured by CRD. The velocity of the HF and LF oscillatory currents are the incident orbital velocities. Positive velocity values denote onshore directed currents.

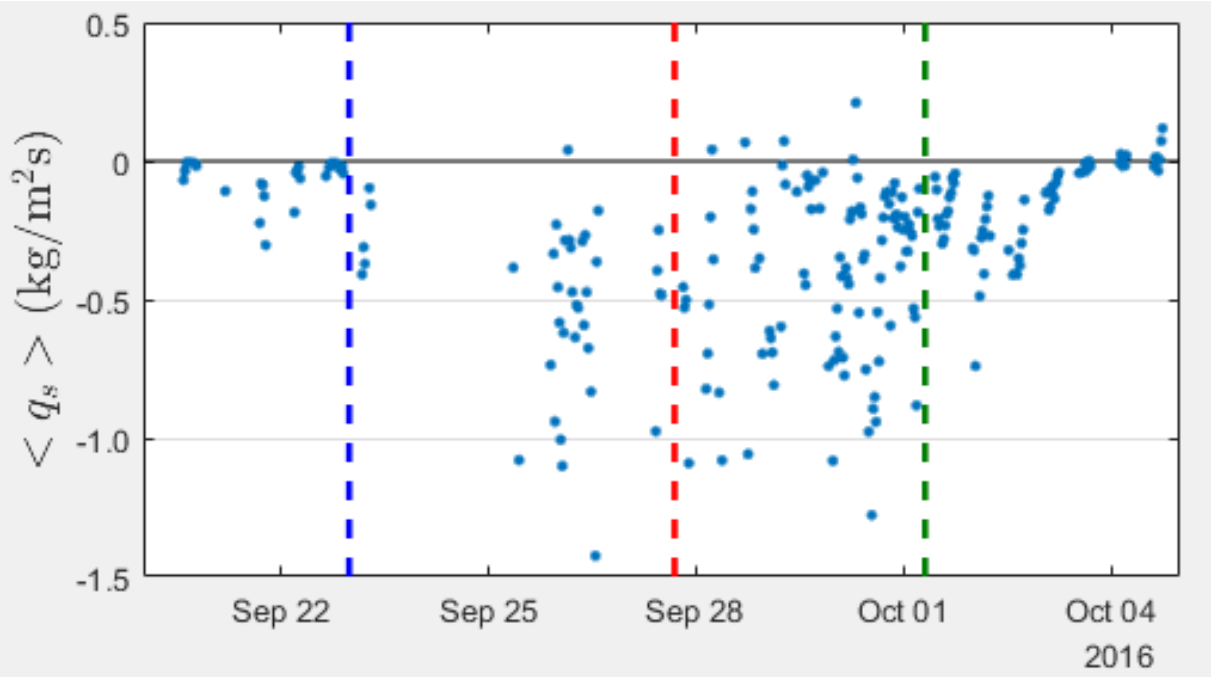

Figure A.2: Time series of net suspended sand transport measured by CRD. The categorisation on the basis of offshore wave conditions and sandbar migration is visualized with the vertical dashed lines. Positive values denote onshore directed transport.

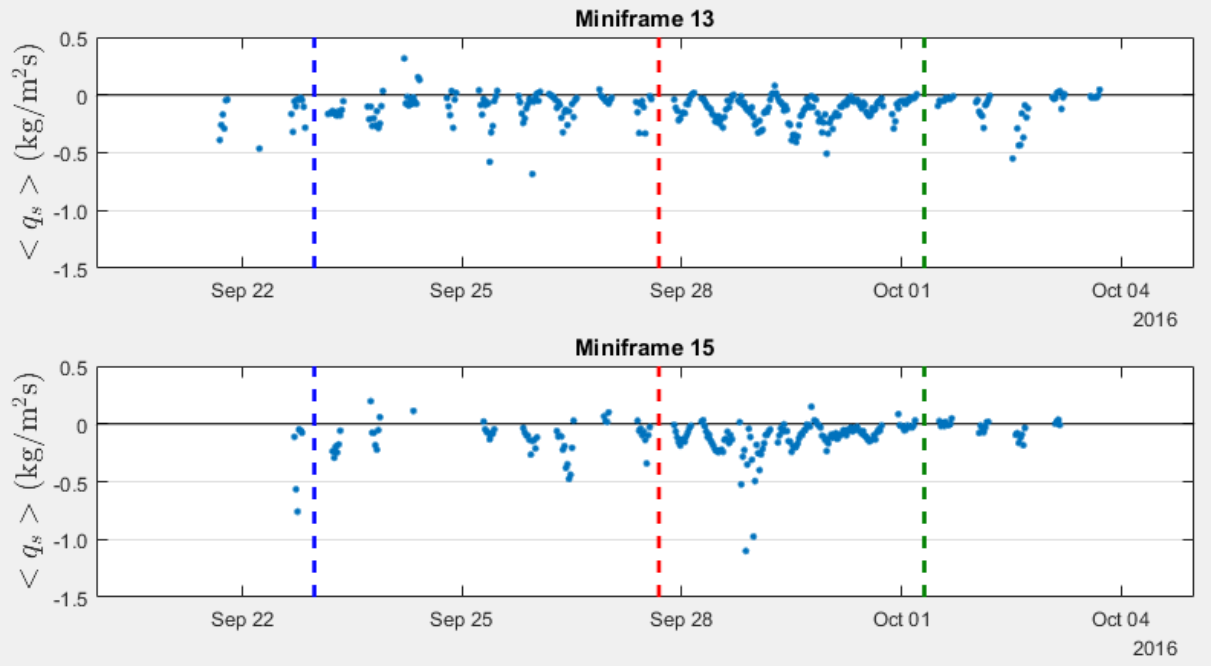

Figure A.3: Time series of net suspended sand transport measured by the two miniframes.

a)

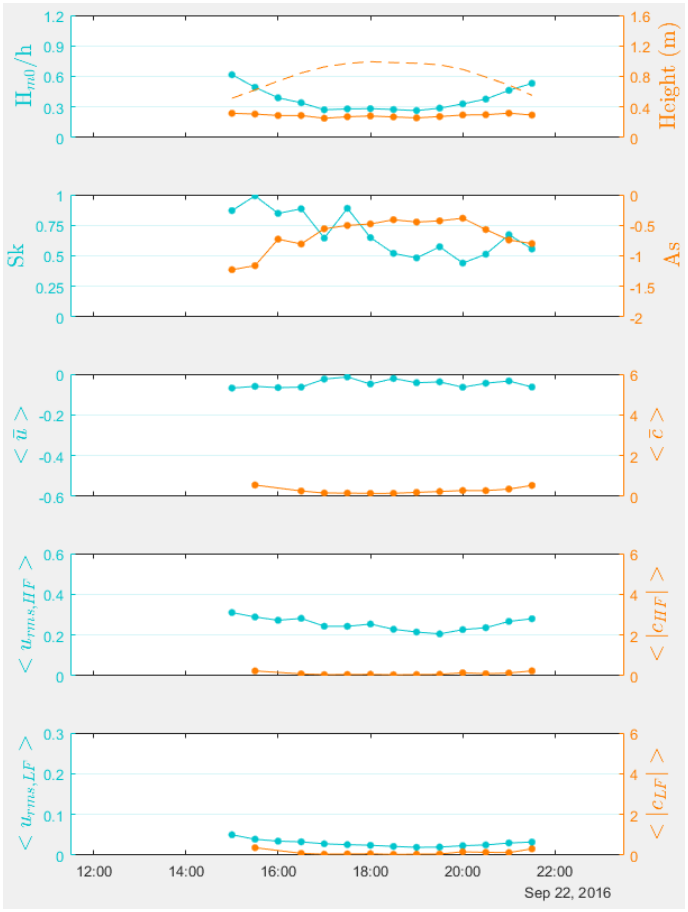

b)

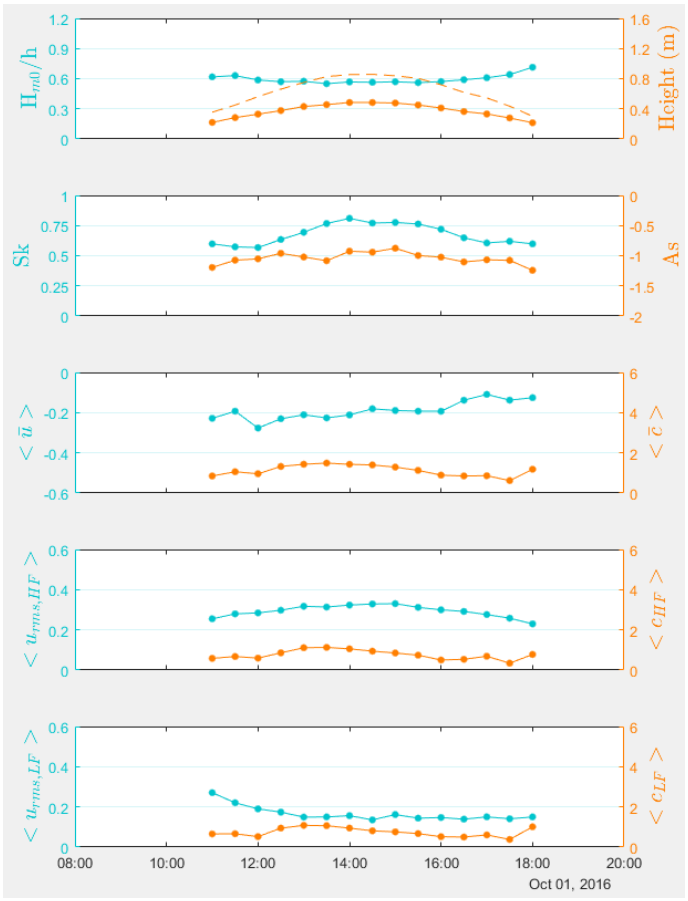

Figures A.4: Temporal change of various hydrodynamical parameters during a single tide in category 1 (a) and category 4 (b). In the first plot wave height is displayed with a solid orange line, water depth with a dashed orange line, and relative wave height is shown in solid blue. The second plot shows skewness in blue and asymmetry in orange. Velocities are in [m/s], with u_{rms} representing root-mean-square orbital velocities. Concentrations are in [kg/m^3].

a)

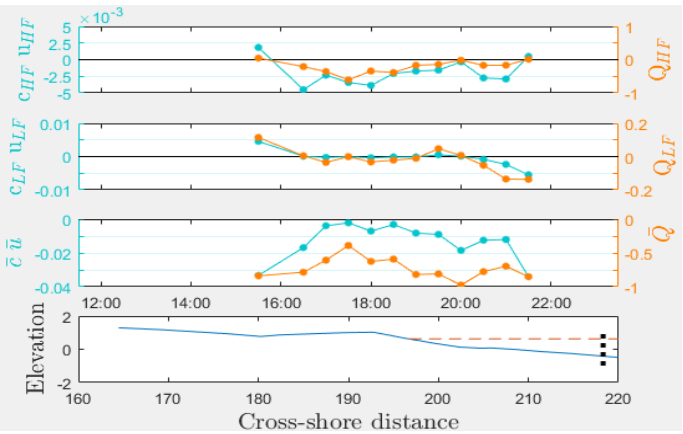

b)

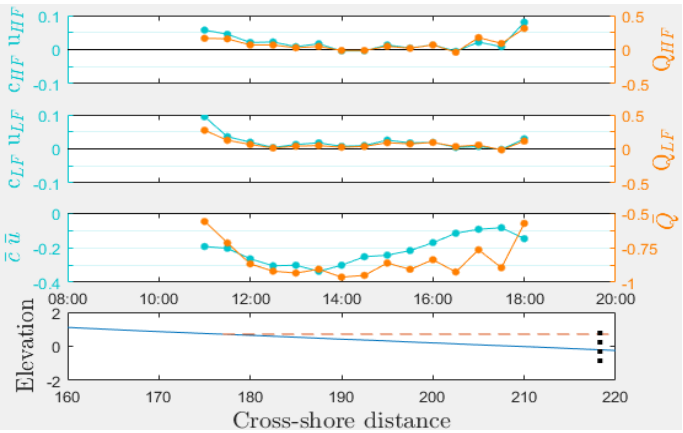

Figures A.5: Temporal change of the magnitude, direction and relative importance of the transport components during a single tide in category 1 (a) and category 4 (b). First plot shows the HF transport component, second the LF transport component and third transport due to steady currents, all with the transport flux in blue and the fraction with respect to the net flux in orange. The last plot shows the corresponding bed profile in blue with the maximum high water level in red. Black dots indicate the cross-shore position of the CRD frame, where the data displayed here is taken from. Transport rates are in [kg/m^{2}s].

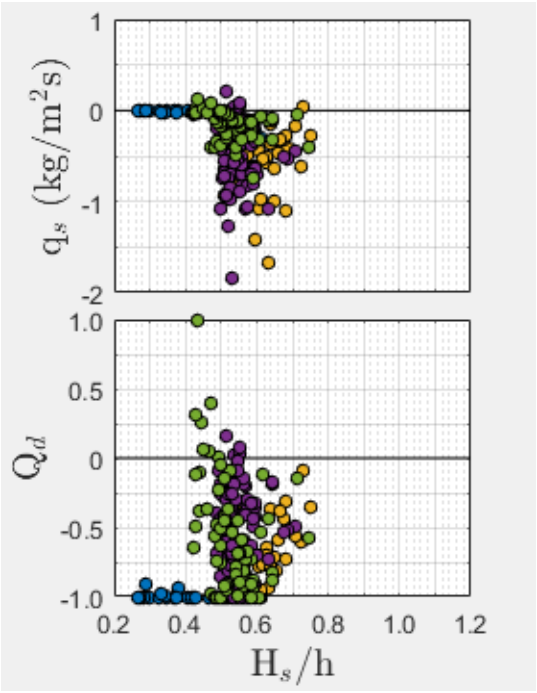

Figure A.6: Net transport rates and net normalized transport index as a function of local relative wave height at the CRD. Colours represent results from the four categories. Transport rates are in [kg/m^{2}s].

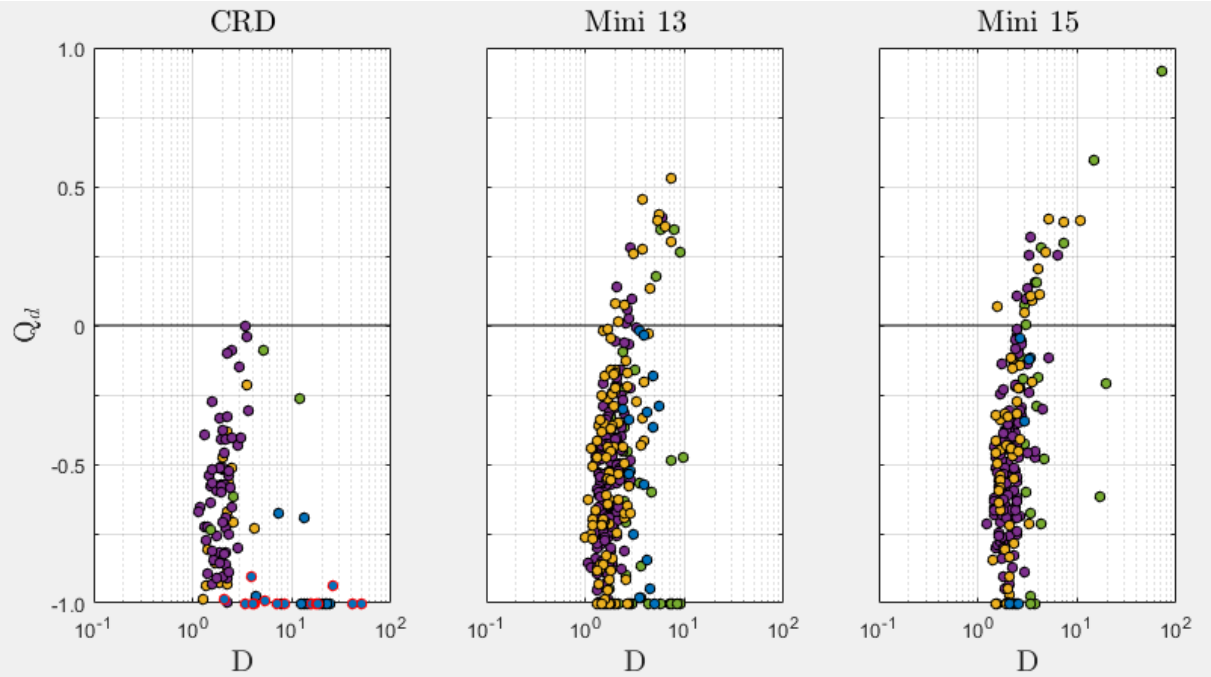

Figure A.7: Net normalized transport index plotted against the non-dimensional parameter D, for the three frames. Colours represent the four different categories.

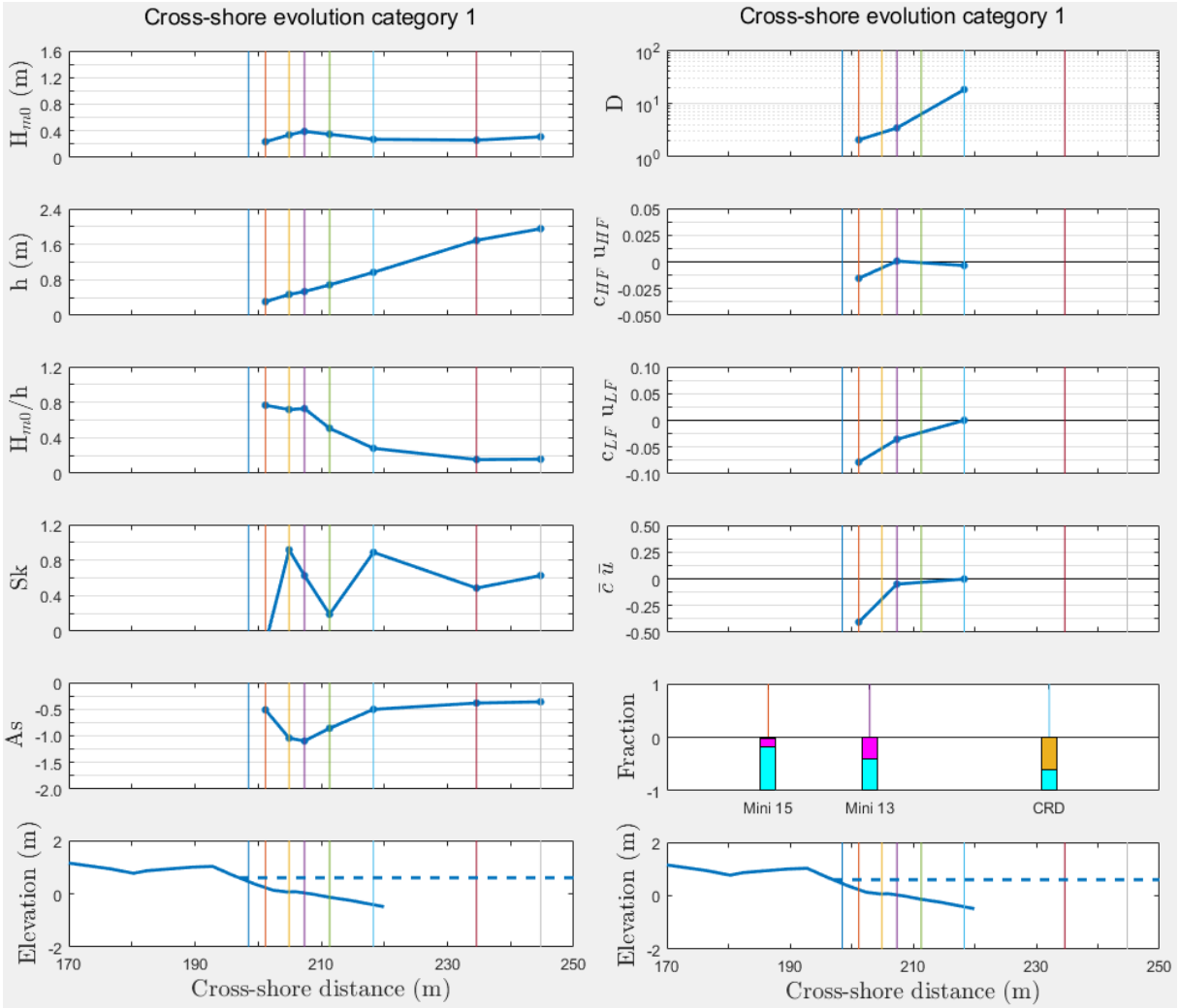

Figures A.8: Cross-shore evolution of hydrodynamical conditions (left) and sand transport (components, right). Line colours represent data from different instants during category 1; Blue: 17:30, 22 Sept. Boxplot colours are orange, magenta and cyan for HF, LF and Steady components, respectively. Transport rates are in [kg/m^{2}s]. Vertical coloured lines indicate the cross-shore positions of the OSSIs and frames (FLTR. OSSI 5, Miniframe 15, OSSI 4, Miniframe 13, OSSI 3, CRD, OSSI 2 and OSSI 1).

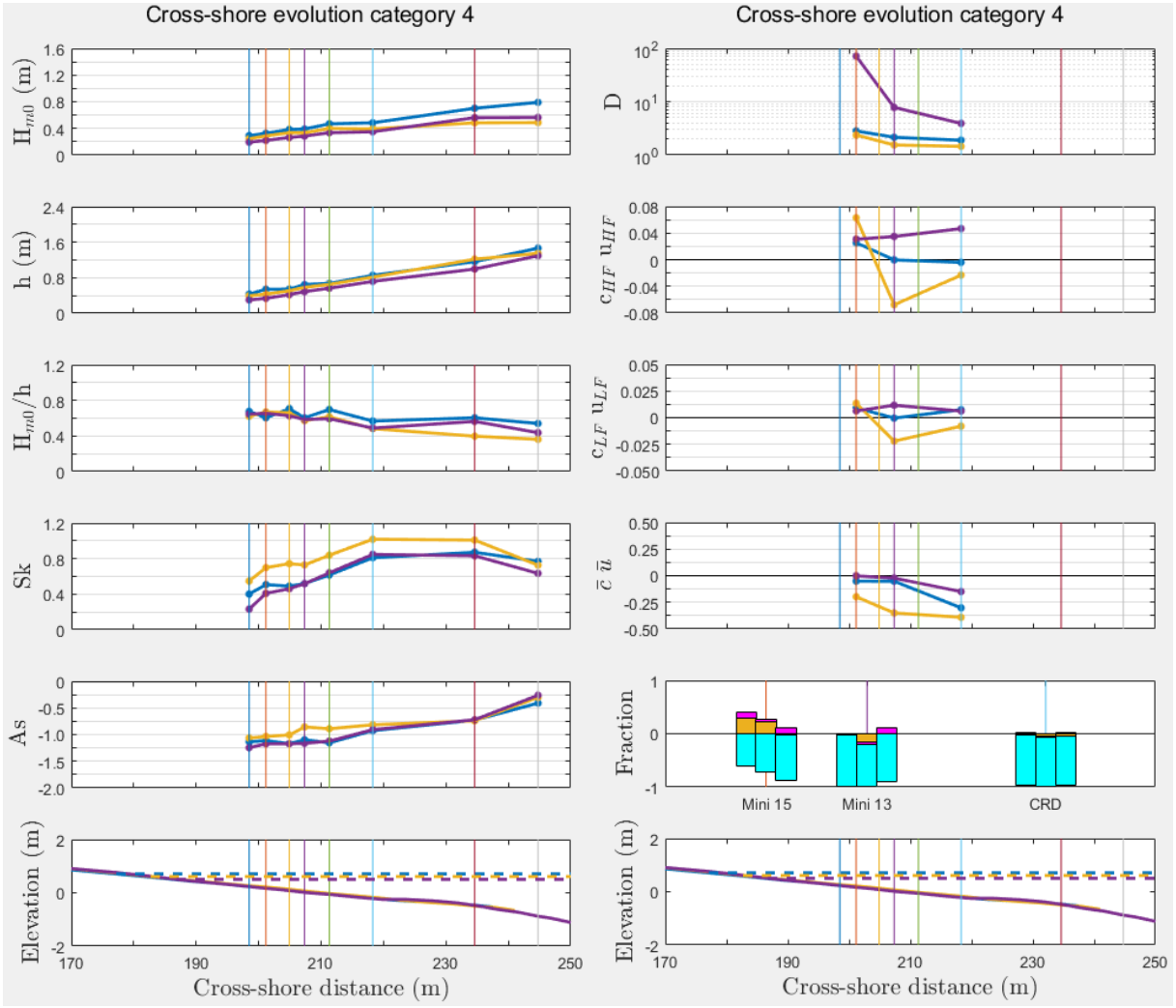

Figure A.9: Cross-shore evolution of hydrodynamical conditions (left) and sand transport (components, right) for category 4; Blue: 14:00, 1 Oct.; Yellow: 15:00, 2 Oct.; Purple: 3:30, 3 Oct.

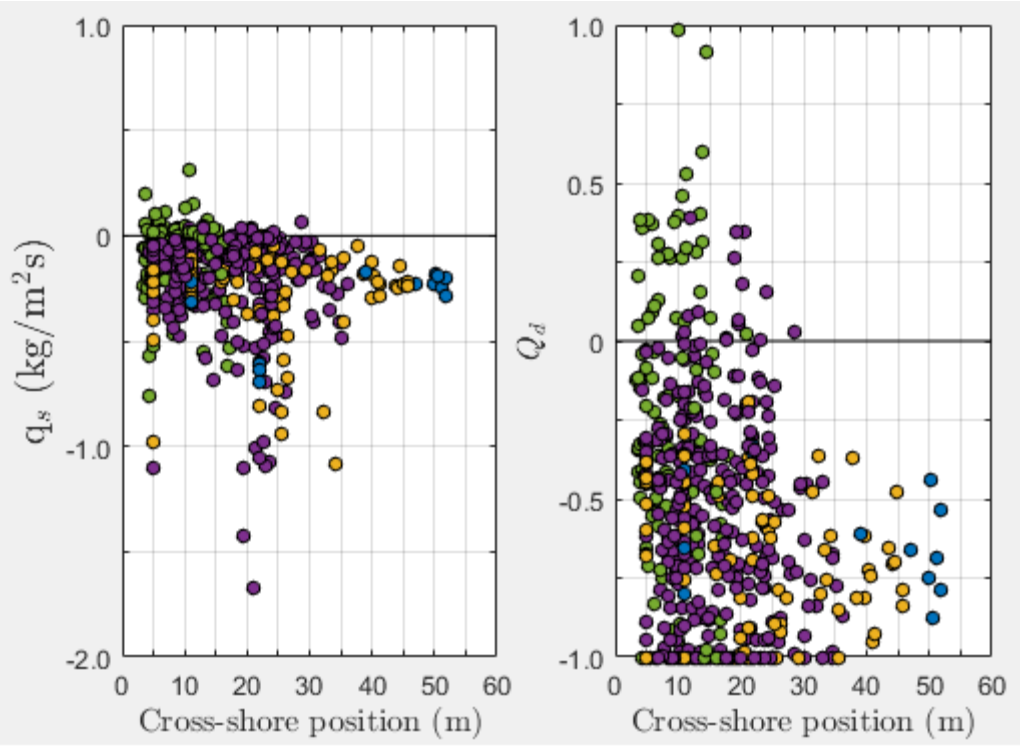

Figures A.10: Dependency of the net transport fluxes and normalized transport index on the cross-shore distance of the three frames. Colours represent the results from the four water level elevation categories.

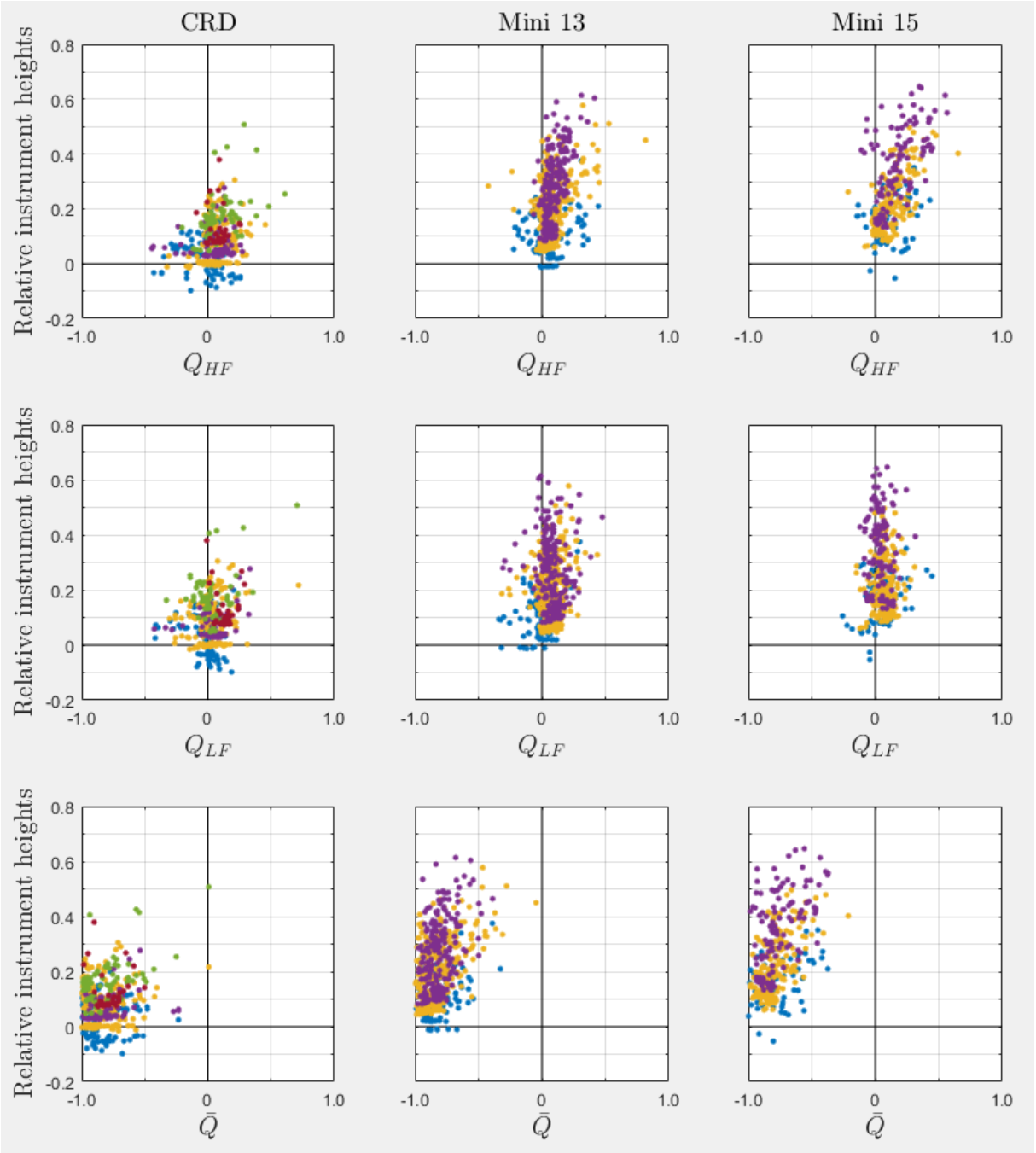

Figure A.11: Vertical profiles of the relative importance of the three transport components for each of the frames. Colours represents data from different STMs/OBSs.

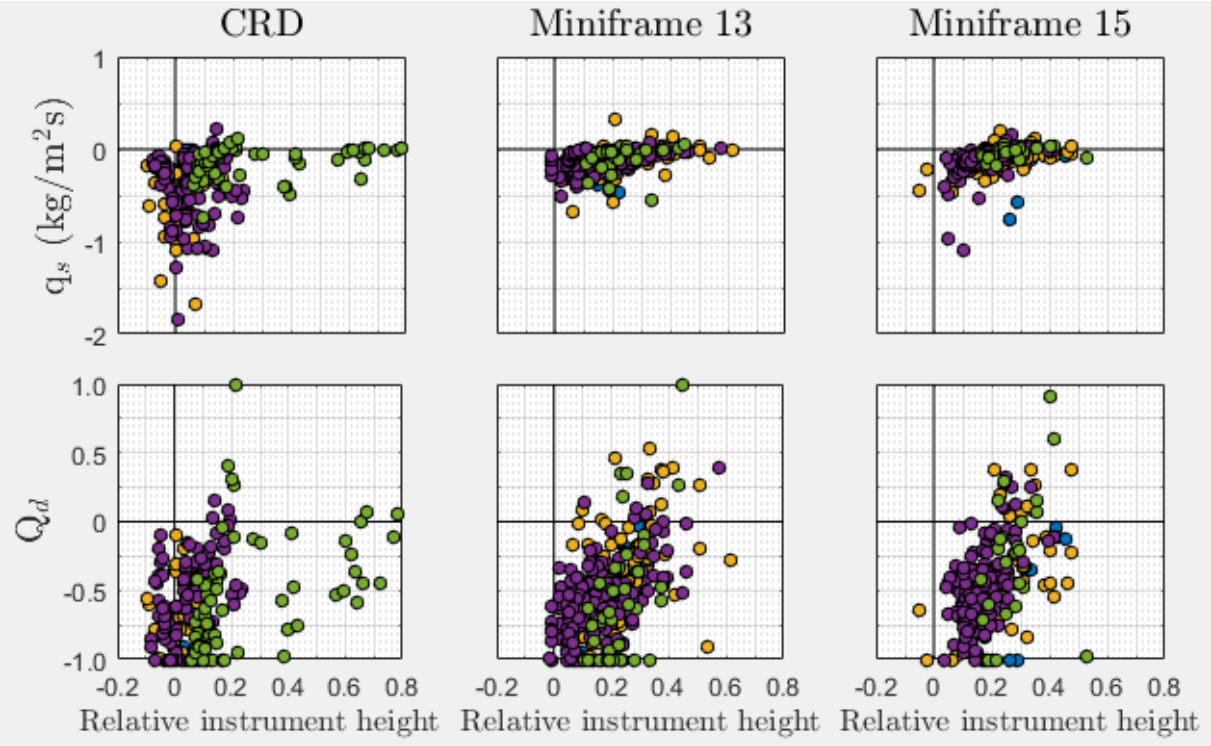

Figure A.12: Net transport and net normalized transport index plotted against relative instrument height for each of the frames. Colours represent the four different categories.